Geotechnical and Geological Engineering (2006) 24: 1307–1348
DOI 10.1007/s10706-005-2023-z

Characterization of a profile of residual soil from granite combining geological, geophysical and mechanical testing techniques

A. VIANA DA FONSECA[1,★], J. CARVALHO[1], C. FERREIRA[1], J. A. SANTOS[2], F. ALMEIDA[3], E. PEREIRA[4], J. FELICIANO[4], J. GRADE[4] and A. OLIVEIRA[4]
[1]*Faculty of Engineering, University of Porto, Rua Roberto Frias, s/n, 4200-465, Porto, Portugal*
[2]*Dept. Civil Engineering, Instituto Superior Técnico, Univ. Técnica de Lisboa, Portugal*
[3]*Department of Geosciences, University of Aveiro, Aveiro, Portugal*
[4]*Instituto Nacional de Engenharia, Tecnologia e Inovação, Porto, Portugal*

(Received 23 February 2005; accepted 10 August 2005)

Abstract. This paper summarizes the results of an experimental site investigation and characterization survey, on a residual (saprolitic) soil from granite, in the framework of a research project led by the Faculty of Engineering of the University of Porto (FEUP). This project aims at characterizing these unusual soils in the context of the development of an International Prediction Event (Class A) on the behaviour of different types of piles. A very extensive site characterization campaign, including a large variety of in-situ tests and field methods, has been held. These investigations comprised the application of several geophysical borehole and surface methods, namely P- and S-wave seismic refraction, reflection, cross-hole (CH), down-hole (DH), electrical resistivity imaging and ground probing radar (GPR), as well as mechanical tests, namely SPT, CPT and DMT, among others. The site is geologically formed by an upper layer of heterogeneous residual granitic soil, overlaying rather weathered granite contacting a gneissic migmatite. Direct and indirect results from some of the referred surveys were compared between them and with some of the available geological and geotechnical information, namely those obtained from seismic, electrical and GPR profiles, conducted adjacent to three boreholes in which undisturbed soil samples were collected previously to geophysical data acquisition. In addition, a comprehensive laboratory testing program was carried out using the collected undisturbed samples. A discussion of the obtained results is hereby presented, giving emphasis to the correlations encountered between the different tests, specific of saprolitic soils with weak relic structures.

Key words. geological, geophysical and geotechnical tests, residual saprolitic soils.

1. Introduction

Residual soils from granite are very common in the northwestern part of Portugal where the ISC'2 experimental site ("site@FEUP") is located, within the campus of the Faculty of Engineering of the University of Porto (FEUP) (Figure 1). Basically,

★ Corresponding author: A. Viana da Fonseca, Faculty of Engineering, University of Porto, Rua Roberto Frias, s/n, 4200-465, Porto, Portugal (E-mail: viana@fe.up.pt).

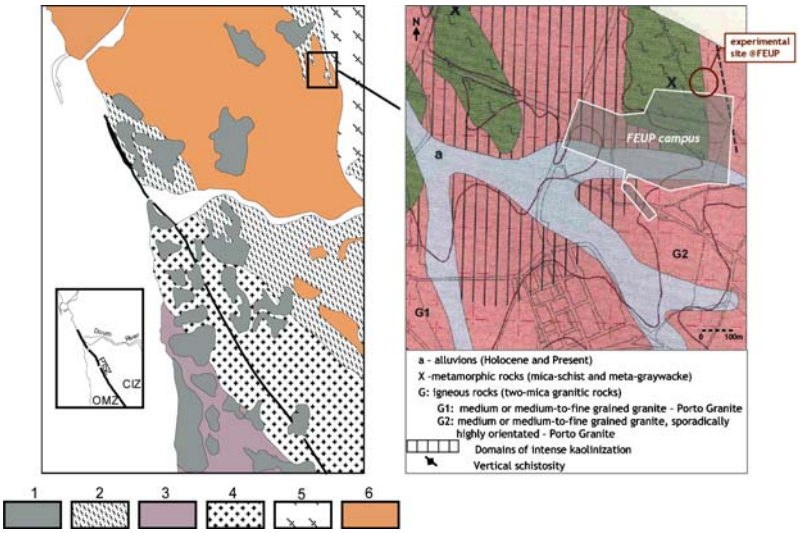

Figure 1. Simplified geological map from Porto area (adapted from Pereira, 1992).

the site is geologically formed by an upper layer of heterogeneous residual saprolitic granite soil of variable thickness, overlaying more or less weathered granite contacting high-grade metamorphic rocks (gneisses and migmatites).

The thickness of these residual saprolitic horizons may vary between few meters to more than 20 m with common values of 5–9 m. Although they generally present strong heterogeneity, it is frequently observed that an average gradual change of characteristics with depth, especially regarding their mechanical properties. Nevertheless, an accurate mapping of the spatial variability of the mechanical properties, necessary for geotechnical design, is often very challenging.

The data compiled during the extensive in-situ and laboratorial investigation and characterization of ISC'2 experimental site, comprising the application of several geotechnical and geophysical surface and borehole techniques, namely SPT, CPT, DMT, surface and borehole seismic, electrical resistivity and GPR, offer a valuable opportunity to compare different methodologies and assess their relative advantages and limitations.

2. Geological Setting and Physical, Chemical and Mineralogical Description of the Profile

Aiming at an accurate understanding of the regional and local geology of the University of Porto experimental site, a brief description of the study, carried out in Instituto Nacional de Engenharia, Tecnologia e Inovação, Porto (INETI) will follow, leading to the characterization of the main cropping out and near surface

geological units and materials. The observation of the simplified geological maps depicted in Figure 1, helps in understanding the geological complexity of the site.

Excluding the thin siliciclastic surface deposits of Cenozoic age, all the other mapped lithologies (granite and metamorphic rocks including high-grade schist, gneiss and migmatite) are part of the basement which is strongly deformed and metamorphosed during the variscan orogeny (Devono-Carboniferous). In fact, the main features of regional geology are mainly due to the variscan orogeny and strongly marked by the closeness to a main tectonic suture between two geotectonic zones: the Ossa-Morena Zone and the Centro-Iberian Zone, which was a major crustal transcurrent shear zone during the variscan times (e.g., Ribeiro et al., 1990). The pervasive metamorphic foliations in the country rocks and, in some extent in the granites, are consequence of these tectonic events.

The schists, gneisses and even migmatites are the metamorphic correspondents of a former thick sedimentary sequence of graywackes, mudrocks and conglomerate levels named Schist and Graywacke Complex. The main granitic body at the site is interpreted as the result of crustal partial melting during the variscan orogeny. The proximity to a major crustal shear zone – the Porto Tomar Shear Zone, an ancient plate boundary of Cadomian age (Ribeiro et al., 2003) that separates the NE Central Iberian Zone from the SW Ossa Morena Zone – and its tectonic activity during the variscan orogeny favoured the crustal melting and the ascent of granitic magmas.

The upper zone of these basement units are frequently strongly weathered, forming often a saprolite level with variable thickness, overlaid by a thin layer of soil and antropic materials, the most common surface and subsurface material in this region. In this Porto area, the fresh outcroppings of basement rocks are rare. In fact, the site is geologically formed by a thin upper layer of soil of varying thickness, overlaying more or less weathered granite (saprolite) contacting an older gneissic migmatite with dominant sub-vertical foliation. This subvertical structural anisotropy can be considered a determining factor to understand the geophysical response of the related residual soils resulting from the weathering process.

2.1. PETROGRAPHY AND PETROCHEMISTRY OF BASEMENT ROCKS

The geological materials identified by the drill-hole cores are very heterogeneous: biotitic gneisses, migmatitic gneisses, gneisses cut by granitic veins and a weathered two-mica peraluminous granite. From these rocks, thin sections of migmatitic gneiss and granite were studied under the polarizing microscope. A sample of unweathered granite was obtained from the same granite massif in an outcrop 600 m south of the experimental site.

2.2. MIGMATITIC GNEISS

This rock shows a typical gneissic foliation with quartz-feldspatic layers alternating with mica-rich layers. The occurrence of thin veins and veinlets of granitic materials

cutting that gneissic structure is interpreted as a sign of the partial melting of the gneiss.

Under the microscope, it is possible to observe a grano-lepidoblastic texture with strong differentiation between quartz-feldspatic domains and biotite domains. A progressive metamorphic process could be deduced based on the formation of silimanite from the biotite (Figure 2) and the genesis of moscovite phenoblasts that cuts the gneissic structure.

The essential minerals present are:

- quartz + oligoclase + biotite;
- silimininanite formed from biotite and moscovite;
- moscovite in phenoblasts;
- K-feldspar formed from Al minerals described above.

Minor mineral phases present in the thin section are: zircon; apatite; iron oxides; phylossilicates resulting from secondary alterations.

The rock is classified as gneiss, in the silimanite + K feldspar zone, in which the process of partial melt is apparent: formation of perthitic K feldspar from the consumption of silimanite and moscovite. Cordierite can occur as a refractary mineral phase:

(i) moscovite + quartz $\rightarrow$ silimanite + orthoclase + H_2O
(ii) moscovite + silimanite + quartz $\rightarrow$ cordierite + orthoclase + H_2O

2.3. TWO-MICA GRANITE

The two-mica granite is a leucocratic medium grain size with sparse megacristals. Despite its sintectonic genesis and installation, the rock is isotropic without any foli-

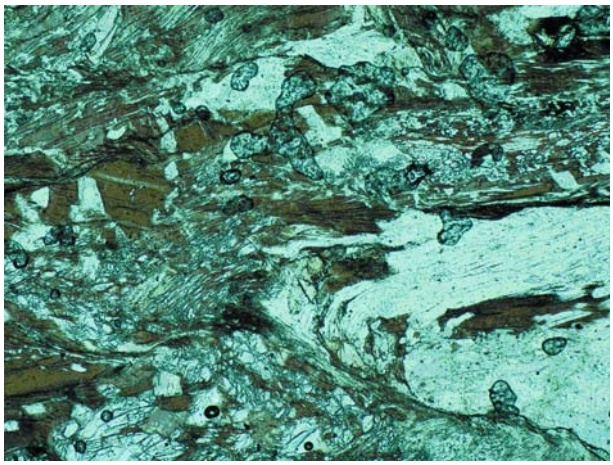

Figure 2. Textural aspect of the formation of silimanite from biotite.

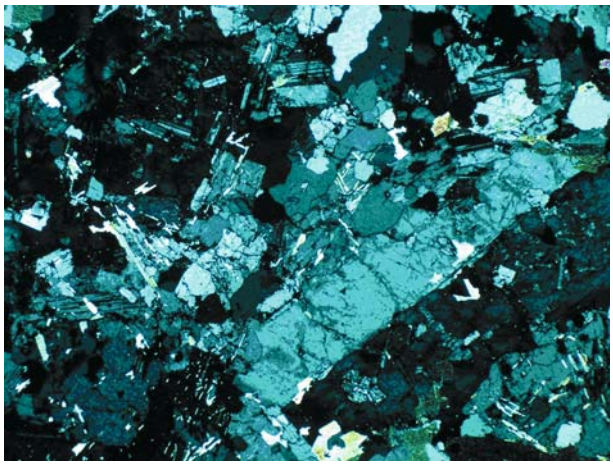

Figure 3. Granular hypautomorphic texture in the granite.

ation. Under the microscope the rock exhibits a granular hypautomorphic texture with the biotite cristals slightly oriented (Figure 3). Some post-magmatic reactions can be seen: a richer primary plagioclase is transformed in lamelar moscovite; in extreme cases, the same plagioclase suffers albitization forming perthitic K feldspar.

When the K feldspar has poekilitic inclusions of albite remains, and then it is anorthose (sodic microcline) that evolves to form microcline-perthite (Figure 4).

Essential minerals are:

- anedric quartz;
- microcline and anorthose;
- two plagioclase types: primary oligoclase and neoformed albite;
- moscovite and rare biotite, sometimes clorithized.

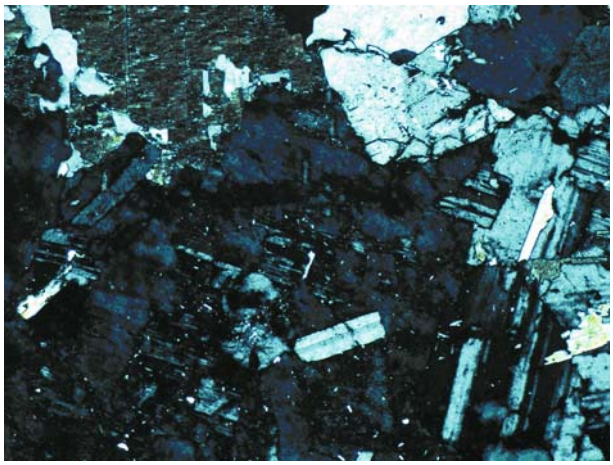

Figure 4. K feldspar with poekilitic inclusions.

Other minerals are present:

- zircon; apatite; Fe, Ti oxides; titanite.

2.4. GRANITE GEOCHEMISTRY

In order to compare the slightly weathered granite (FE2), collected away from the experimental site, with the weathered granite (FE1), obtained at the experimental site from drill-hole cores, chemical analysis of major and minor elements were made. Table 1 synthesizes the values of the major elements as well as the incompatible elements.

The most distinctive differences between the values of the analyzed elements are found in the LOI. This is due to the fact that the weathered granite has a high percentage of clay minerals resulting from the weathering of feldspars. These clay minerals include significant amounts of H_2O in its structure that volatilize during the LOI test. Among the feldspars, the plagioclases are more affected by weathering than the microcline and the anorthose, which is expressed by the loss of CaO and Na_2O as well as by the loss of incompatible elements such as Ba and Sr, present in the plagioclase structure.

Nevertheless, all these chemical variations due to weathering are not significative when discriminant diagrams are employed to determine the geotectonic environment of granite genesis. In Clarke's classification scheme, the referred rock samples being compared are both plotted in the field of peralluminous granites. This fact clearly means a genesis from the partial melting of crustal materials, rich in metassediments and consequently in alumina (Figure 5a).

In addition, the crustal genesis of these granites is also suggested by the profile of incompatible elements. In Figure 5b, the enrichment of large ion lithofille elements (LIL) and depletion in high-field strain elements (HFS) is clear.

The strong crustal contribution in the genesis and evolution of the granitic magma can be highlighted by the fact that the amount of incompatible elements LIL is higher than the amount of incompatible elements HFS, when compared with a primitive material of chondritic composition.

Finishing this brief petrochemical analysis on granitic composition, it could be pointed out that the use of the Pearce diagram (Pearce et al., 1984) is very elucidative (Figure 6).

This diagram allows relating the following geodynamic environments to the genesis of granitic rocks: intraplate (WPG); magmatic arc related with subduction (VAG); hybridisation during orogenic processes (ORG) and genesis of granitic magmas by colisional processes (syn-COLG). Despite the strong weathering and lixiviation of mobile lithofile elements in the FE1 sample from the experimental site, its characteristics of a peraluminous colisional granite persist unaltered. In fact, the plots in the Pearce diagram confirm the hypothesis of a granite formed by a continental collision in the internal part of the orogen during the peak of metamorphism,

Table 1. Major and minor element chemical analysis of the two-mica granite (INETI Laboratory – Porto)

Samples	Major elements (%) – XR Fluorescence										
	SiO_2	Al_2O_3	Fe total	MnO	CaO	MgO	Na_2O	K_2O	TiO_2	P_2O_5	LOI
FE1	69.59	17.72	1.87	0.05	0.19	0.44	1.13	4.38	0.27	0.13	4.02
FE2	71.90	15.50	1.55	0.02	0.30	0.33	2.95	4.66	0.19	0.41	1.95
Samples	Minor elements (ppm) – XR Fluorescence										
	Rb	Sr	Y	Zr	Nb	Ba	Ta	Sn	Th		
FE1	204	84	10	117	5	512	< 15	19	13		
FE2	357	38	4	64	7	160	< 15	22	11		

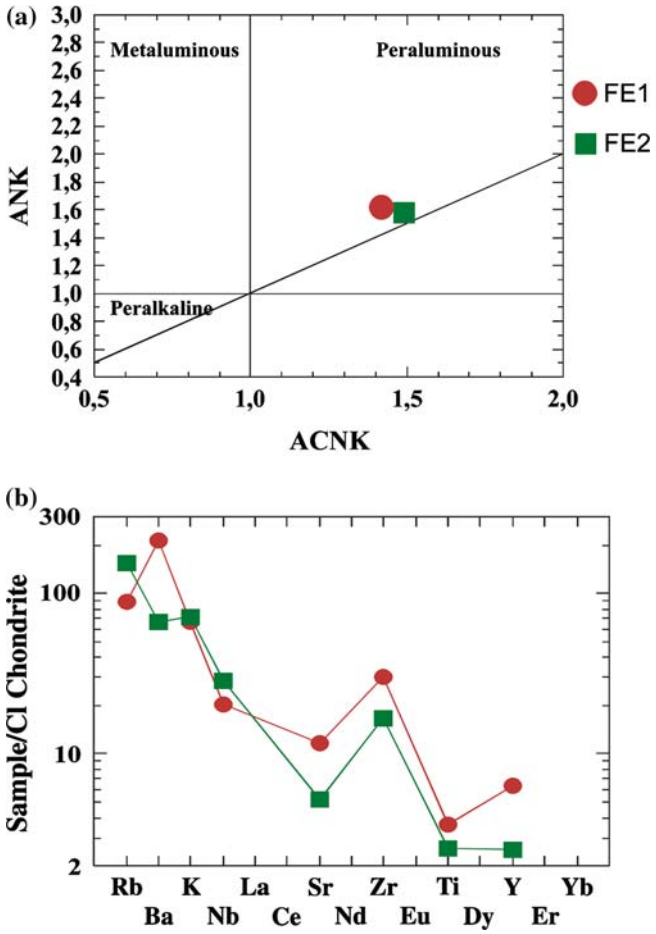

Figure 5. (a) The weathered granite (FE1) and fresh granite (FE2) samples show their similarities in this diagram. Both rocks are located in the field of peraluminous granites with A/CNK > 1; (b) The samples of weathered granite (FE1) and fresh granite (FE2) have similar profiles of incompatible elements, revealing a strong crustal contribution in their genesis.

by the partial melting of both existent metassedimentary materials and granites formed during a former orogenic cycle.

2.5. STRUCTURAL DATA OF METAMORPHIC ROCKS

An intense planar anisotropy (gneissic foliation) can be observed in local drill-hole gneissic cores having an orientation in accordance with the known NW–SE strike and 60° eastwards dipping of the regional variscan structure.

The 1:50,000 Porto geological map shows a clear contact line between the gneissic metassediment and the granitic mass. In this complex structural and metamorphic zone, it is admitted that the type of regional transition between the two bodies is not

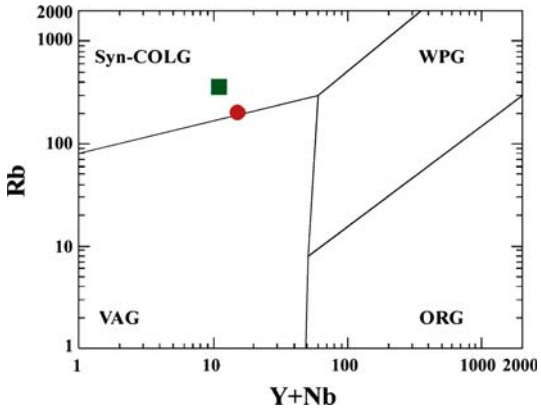

Figure 6. Weathered granite (FE1) and fresh granite (FE2) plot in Pearce et al. (1984) diagram.

a single discontinuity surface but rather gradual, consisting of an eastward "probabilistic" decreasing of feldspar bands maintaining the local trend of geological planar anisotropy. Nevertheless, locally, there are zones of sudden lithologic changes.

2.6. WEATHERED MATERIALS

The differences in the weathering processes of granites and gneisses are the main factor for the irregular weathering profile of these rock formations, leading to a quite irregular spatial distribution.

As previously mentioned, in general, the thickness of these residual granitic soils (saprolitic formations) varies from a few meters to, sometimes, more than 20 m with more common values of 5–9 m.

Some samples were taken from the borehole cores to study the weathered materials, in particular the changes in grain size and mineralogy with depth. The following was obtained:

- *Mineralogical analysis* (<2 μm fraction): The mineralogical semi-quantitative results obtained by DRX are summarized in Table 2.

The values in Table 2 are typical of a weathered granite mineralogy. Kaolinite is the dominant mineral and mica is, as usual, the second mineral. Some samples from borehole S3 are an exception, where quartz replaces mica as second mineral. Accessory minerals, such as K feldspar, Na feldspar and hematite, are the remaining minerals.

- *Grain size analysis*: Grain size analyses were carried out using a laser beam particle size analyser (Coulter LS130) and by wet sieving. The results are presented in Table 3 and graphically summarized in Figure 7.

In Figure 8, mineralogical and textural data are considered.

Table 2. The mineralogical semi-quantitative results obtained by DRX

Depth (m)	Mica (%)	Chlorite (%)	Illite-chlorite (%)	Kaolinite (%)	Quartz (%)	K Feldspar (%)	Na Feldspar (%)	Hematite (%)
Borehole 1								
0.10–1.70	15	–	2	79	1	–	–	3
1.80–2.75	15	–	–	83	–	–	–	2
3.00–3.65	15	–	–	83	1	–	–	1
4.50–7.15	45	–	–	54	–	–	–	1
7.50–9.65	34	–	–	65	1	–	–	–
9.75–12.65	11	1	3	84	1	–	–	–
12.80–12.95	11	1	1	86	–	1	–	–
13.50–13.65	27		2	68	1	1	1	–
13.75–16.65	25		2	69	1	1	1	1
16.75–19.60	26	1	2	68	1	1	1	
Borehole 3								
0.3–2.2	15	–	3	79	2	–	–	1
2.45–3.7	12		–	65	21	1	–	1
5.5–5.95	14		–	77	8	1	–	–
6.2–7.9	5		3	66	25	1	–	–
8.15–10.95	5	2	3	78	12	–	–	–
11.2–12.7	5	–	3	90		1	–	1
12.95–16.7	8	–	3	80	8	1	–	–
16.95–21.1	15	3	3	72	7	–	–	–

2.7. SUMMARY OF THE GEOLOGICAL CHARACTERIZATION OF THE WEATHERED MATERIALS

The results of the grain size analyses show that both clay and silt particles decrease with increasing depth whereas the sand particle size increases with depth. These facts are more relevant in the samples of borehole S3.

Concerning the clay fraction mineralogy, kaolinite is the main mineral. However, a slight decrease in its quantity is observed with increasing depth. This fact is in agreement with rock weathering. The high quantity of quartz in borehole S3, when compared with borehole S1, suggests different (degrees) of weathering. The chloritization of micas is more important in the rock sample from borehole S3. It is worth mentioning the probable existence of a percolation level at 12.7 m in borehole S3 and at 12.9 m in borehole S1 suggested namely by the increasing kaolinite at these depths.

3. Geophysical Survey

A very extensive site characterization campaign has been held, including a large variety of geophysical borehole and surface methods, namely P- and S-wave seismic conventional (RC) and tomographic (RT) refraction, high-resolution shallow reflection, cross-hole (CH), down-hole (DH), electrical resistivity imaging and ground probing radar (GPR).

Table 3. The mineralogical semi-quantitative results obtained by DRX

Depth (m)	<2 μm	2–63 μm	>63 μm
Borehole 1			
0.10–1.70	8.24	41.59	50.17
1.80–2.75	5.03	29.11	65.86
3.00–3.65	5.79	30.10	64.11
4.50–7.15	4.55	29.91	65.54
7.50–9.65	4.56	29.00	66.44
9.75–12.65	4.07	30.23	65.70
12.80–12.95	3.17	26.35	70.48
13.50–13.65	3.34	20.52	76.14
13.75–16.65	2.37	23.83	73.80
16.75–19.60	3.02	24.25	72.73
Borehole 3			
0.3–2.2	7.39	38.33	54.28
2.45–3.7	3.52	19.64	76.84
5.5–5.95	2.64	14.76	82.60
6.2–7.9	2.47	13.85	83.68
8.15–10.95	1.92	13.08	85.00
11.2–12.7	2.08	13.39	84.53
12.95–16.7	1.40	10.50	88.10
16.95–21.1	0.50	4.61	94.89

Direct and derived results from the applied methods and techniques were compared between them, as well as with some of the available geological and geotechnical information (Carvalho et al., 2004; Almeida et al., 2004).

The generic layout map of the site (Figure 9) shows the location of the seismic, electrical and GPR traverses, around 50 m long, conducted adjacent to three boreholes, S1, S2 and S3, in which undisturbed soil samples were collected prior to geophysical data acquisition.

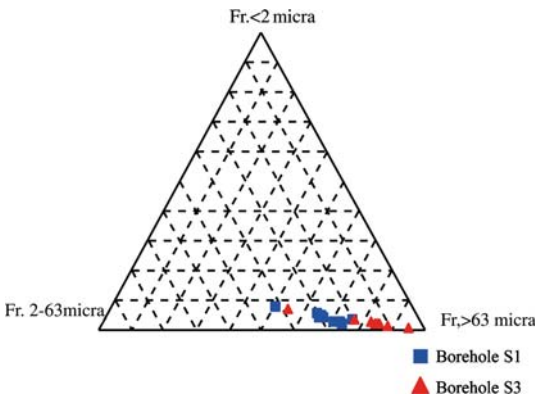

Figure 7. Grain size analysis.

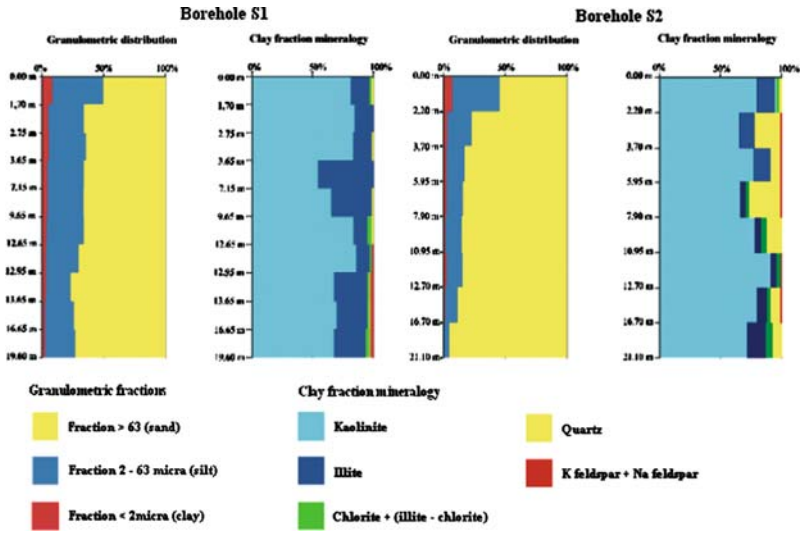

Figure 8. Mineralogical and textural profiles for borehole S1 and borehole S3.

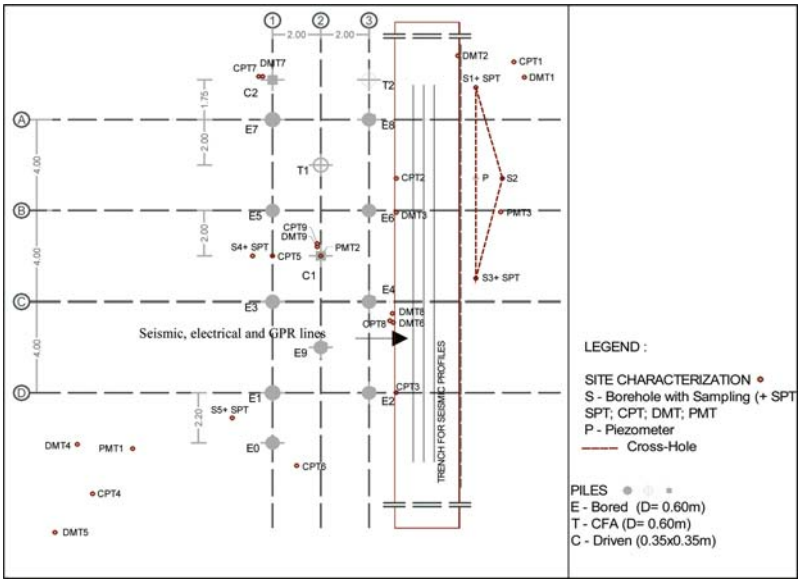

Figure 9. Layout of ISC'2 experimental site.

The CH survey took place between boreholes S1–S2, S2–S3 and S1–S3. In borehole S3, a DH survey was conducted.

3.1. SURFACE METHODS

Seismic refraction data acquisition was performed along a 44.5 m long traverse, having 1.5 m meter spacing between geophones and nine shot points. The generic

S-wave (Figure 10) and P-wave travel time pattern, points out to an average gradual increase of velocity with depth.

The conventional delayed time interpretation was done with software SIPT2 provided by Rimrock Geophysics® and the tomographic inversion was performed with the software SeisOpt22D provided by Optim software®. The corresponding S-wave velocity (V_S) values are consistent for both models and with those obtained from CH and RT.

The P-wave velocity (V_P) section resulting from tomographic inversion is presented in Figure 11 and Figure 12 shows the V_S section resulting from tomographic inversion, overlaid by the obtained time delay method three layers model (dotted lines).

The overall pattern of velocity variability matches the one obtained with electric resistivity imaging: two traverses using the pole–pole method were developed parallel to the seismic refraction traverse and one of the resulting sections from the inversion interpretation method is shown in Figure 13.

In both seismic and electrical interpretations, a sub-vertical "contact" appears on the right side of the section separating zones of overall different seismic velocities and apparent resistances. The lower value zone, on the right side, corresponds to a higher seismic velocity zone signed by RC sections and confirmed notoriously in RT S-wave section.

The high-resistivity anomaly above water level (referred above) is interpreted as being related to a lesser kaolin band dipping 60° eastwards. The high RT V_S zone (also referred above) is well correlated with that high-resistivity anomaly. The lower

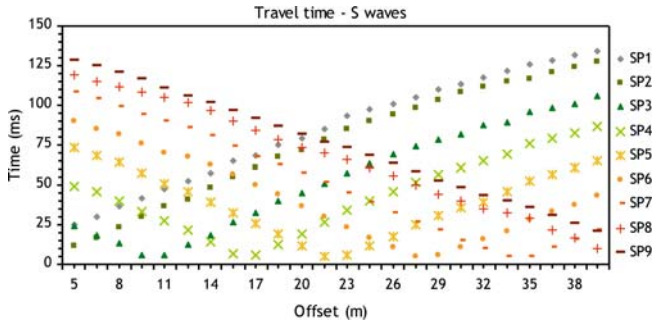

Figure 10. Refraction S-wave travel time plots.

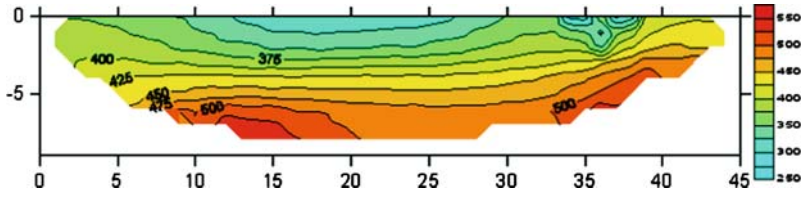

Figure 11. Refraction tomography P-wave model.

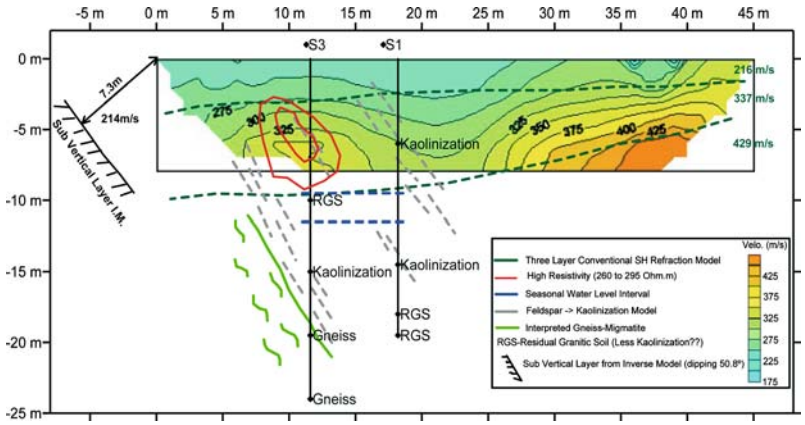

Figure 12. Refraction tomography SH velocity model overlaid by geophysical results (Carvalho et al., 2004) and geological model used for seismic reflection interpretation (Almeida et al., 2004).

V_S zone in the middle of the profile is interpreted as a clayey band due to the fact that V_P do not change significantly along the horizontal direction therefore, within this lower V_S zones, the Poisson's ratio will increase to a clayey domain.

The RC method shows two interfaces (dotted lines in Figures 12 and 14) where velocity changes: the lower one is interpreted as being related to seasonal water level and the upper one is very consistent namely with the tomographic and reflection velocity fields (Figures 11 and 13) as well as with GPR results (Figures 14 and 15). In the processed radargram (Figure 14) a reflector with very good agreement with the RC model first interface is visible; the N_{SPT} values increase between 3 and 4 m deep which supports the existence of a transition zone. There are some visible diffractions, and a possible less weathered zone between 0 and 5 m along the transect line and from the surface to 3.5 m depth.

In order to evaluate the response of the site to reflected S-waves, a reflection profile was done after a walk way noise test.

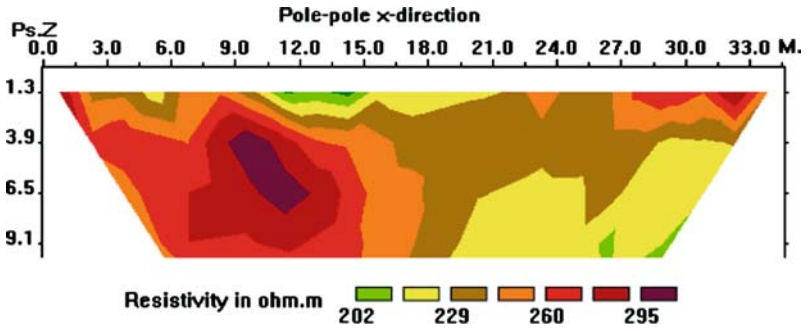

Figure 13. Electric resistivity image.

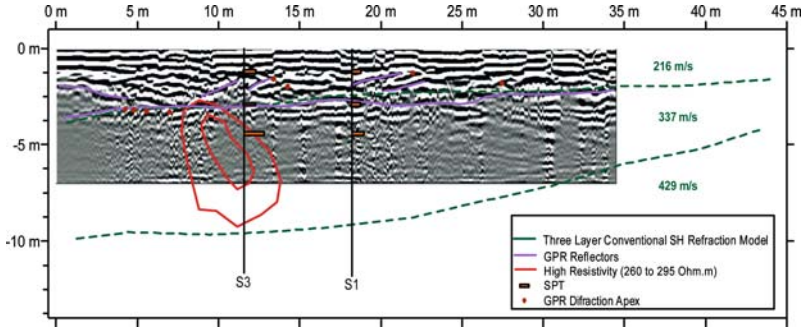

Figure 14. Processed radargram with interpreted events overlaying the resistivity and CH model and N-SPT values in boreholes S3 and S1.

For this test two Seistronix Ras24 seismographs were used, having 24 and 12 available channels. The 28 Hz horizontal geophones spacing was 0.5 m and minimum offset 1 m with a sampling interval of 0.25 ms. In order to obtain a record with 72 channels, the system was rolled over once, five stacks for each polarity were used and the shot was at the starting point of the seismic line.

Following the processing procedures, the next step was to overlay all the information interpreted from seismic reflection, refraction, resistivity, GPR and from the geology (Figure 15).

In Figure 15a, the interval velocities obtained from CMP analysis are overlaid by the RC three layers model, the high-resistivity contour lines and the hypothetical lateral dipping structure model (dip: 50.8°E) obtained from seismic side reflections. This model is believed to be related to the identified 60°E dipping gneissic-migmatite local structures. In Figure 15b the seismic stacked section obtained is overlaid with interpreted seismic and GPR information.

3.2. BOREHOLE METHODS

Three boreholes, S1, S2 and S3 (Figure 9), were used for S- and P-wave seismic CH and DH surveys. CH data acquisition took place between boreholes S1–S2, S2–S3 and S1–S3 and in borehole S3 a P- and S-wave DH survey was conducted, with a 1.5 m interval between shots. These tests were carried out in July, during the dry season, with 10 m deep groundwater level. V_S and V_P variability with depth can be seen in Figure 16 corresponding to CH sections S3–S2, S2–S1 and S3–S1 and to the corresponding RT "CH" sections, CHRT. There is, also in this case, a good agreement between CH and CHRT sections. Derived geotechnical parameters from the CH and DH seismic results will be presented below.

The fact that the P-waves CH detected clearly the presence of water around 3.5 m below the piezometer measurement was associated to the high sensitivity of P-waves to total saturation and in less degree to the presence of moist. Conversely, the water level presence distinctive sign may be the transitory decrease in both P- and S-wave velocity starting at 10.5 m.

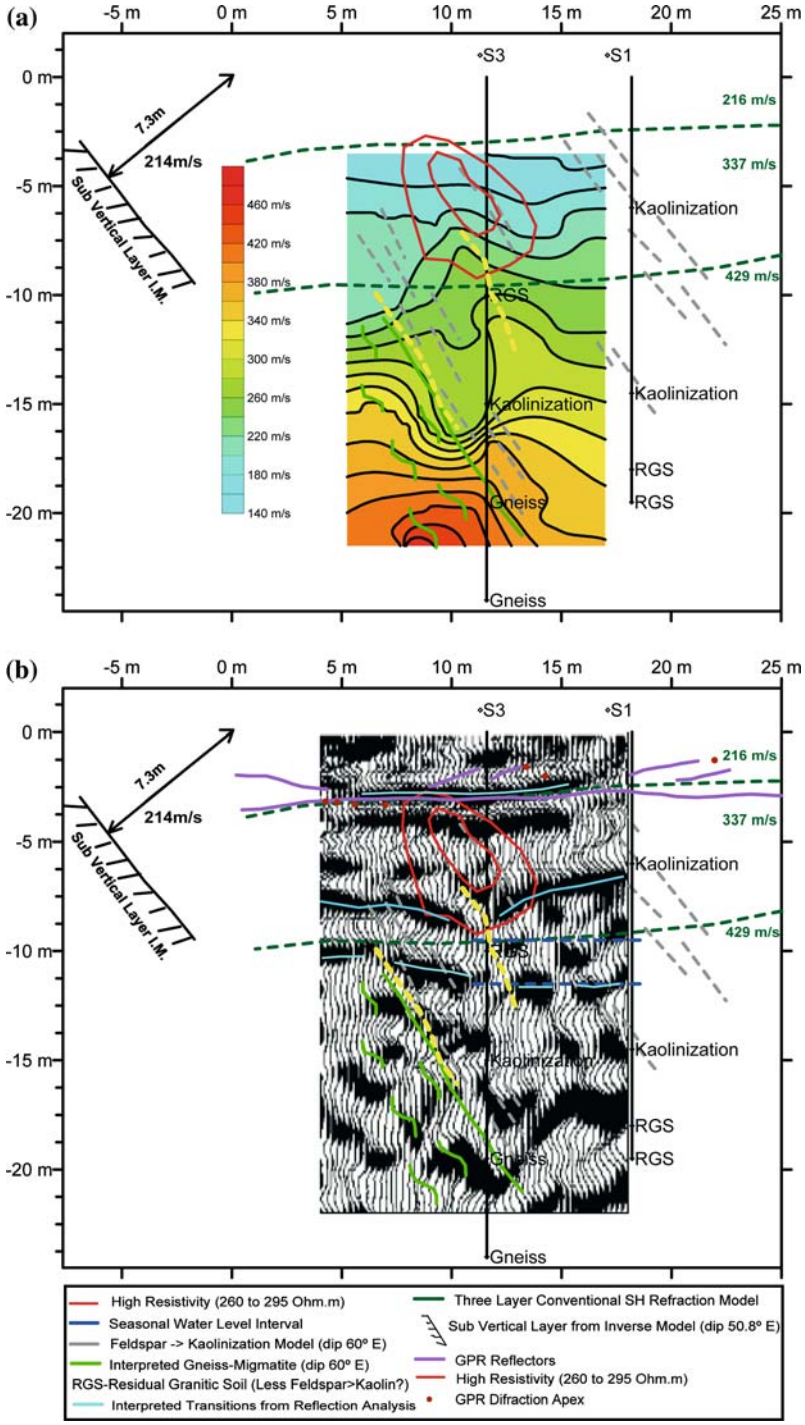

Figure 15. Integration of the interpreted partial models: (a) interval velocity model; (b) stacked seismic reflection section.

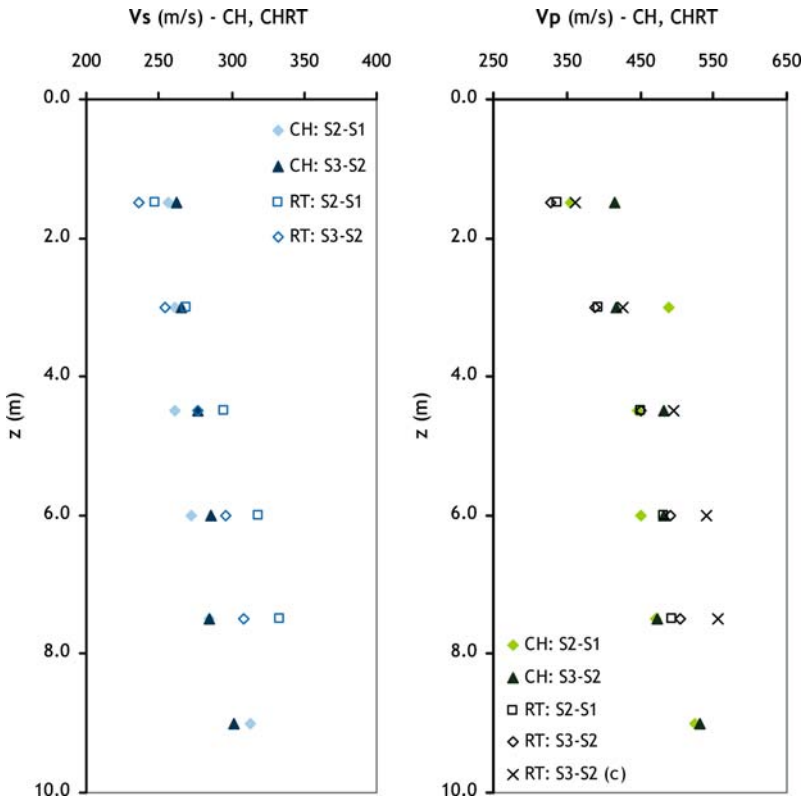

Figure 16. V_S and V_P from CH and tomographic refraction (CHRT) sections.

4. Geomechanical Characterization

4.1. DERIVED PROFILE AND RESULTS FROM IN-SITU MECHANICAL TESTS

In spite of the natural spatial variability of the fabric of these residual soils due to some preserved relic heritage, there is evidence of a fairly homogeneous ground profile in geotechnical terms, as demonstrated by the results obtained with continuous sampling from drilling, with the SPT sampler – schematically shown in Figure 17 with photos of samples obtained from borehole S3 – and from high-quality samplers (Viana da Fonseca et al., 2004).

The first stage of site characterization included 4 SPT, 5 CPTU, 5 DMT, 3 PMT and several CH, DH, SASW and CSWS, while in the second stage 4 CPTU and 4 DMT were performed. The technical data of the first stage of in-situ tests is summarized in Figures 17–19. As referred above, three boreholes (S1, S2 and S3 – Figure 9), were used for S- and P-wave CH survey. Derived values of the shear modulus, G_0, and Poisson's ratio, ν, are included in Figure 19.

As expected, G_0 and V_S variability with depth follows a similar pattern, generally smooth, although more erratic in the case of DH based values. The ν values show in

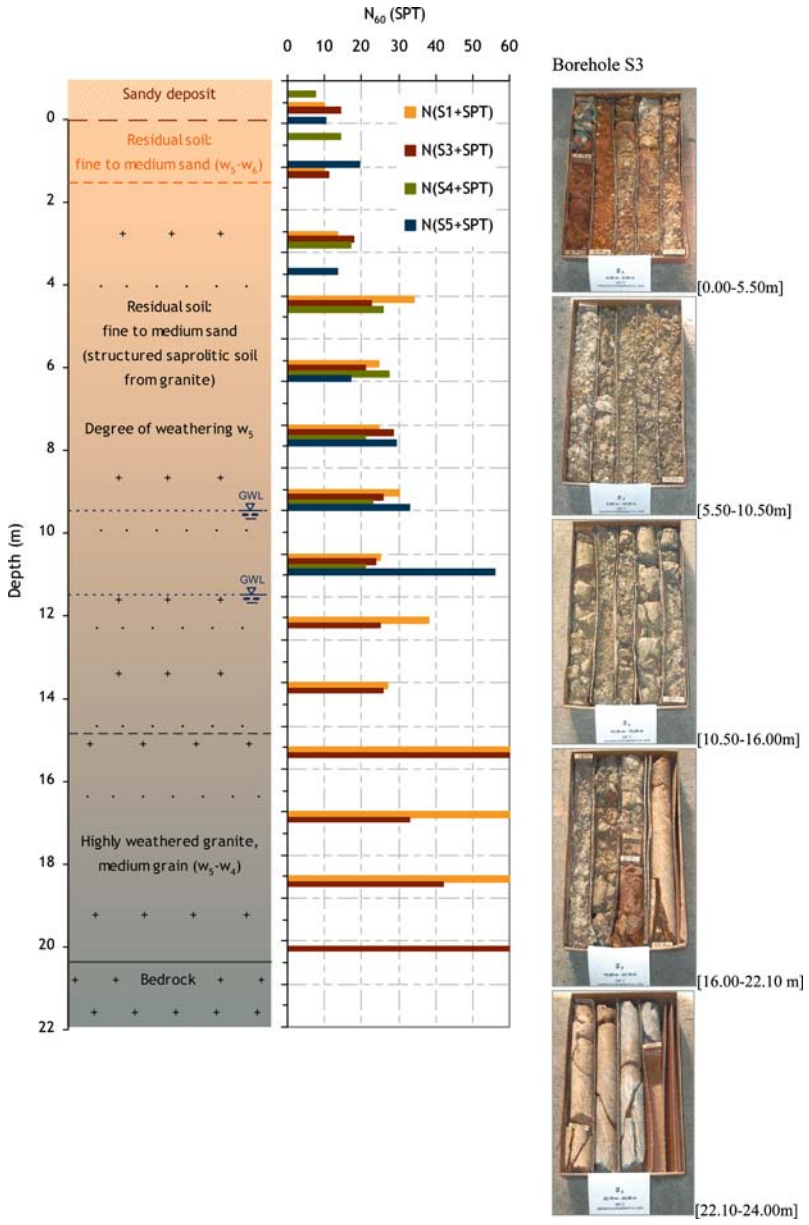

Figure 17. Geotechnical profile and photos of the samples obtained in boreholes (S3 – Figure 9).

general higher dispersion, except in the saturated zone below 13.5 m. While in the zone above 13.5 m, the values vary around an average value of 0.25, below that level these are quite constant with values near 0.5 (around 0.48).This is an obvious sign of full saturation.

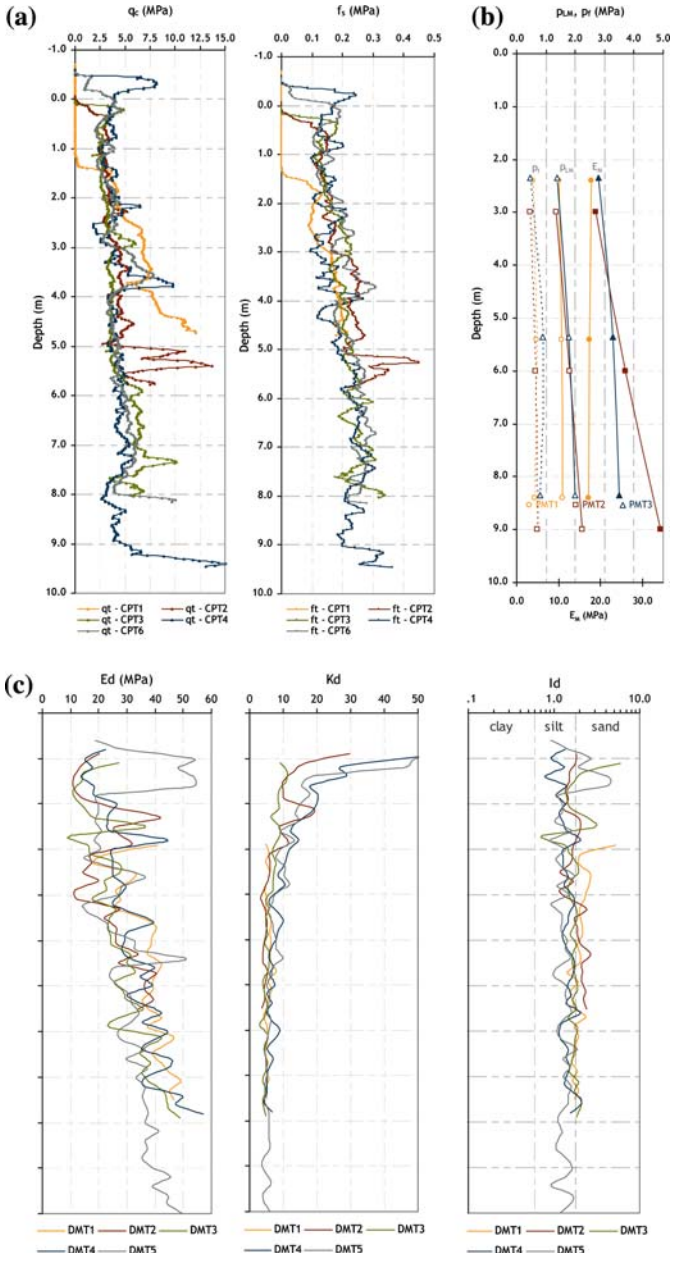

Figure 18. In-situ tests profile: (a) CPTU: q_c and f_s; (b) PMT: p_f, p_{LM} and E_M; c) DMT: E_d, K_d and I_d[1].

G_0 and ν values down to 9 m – the zone of highly weathered saprolitic soil – are plotted in Figure 20. V_S values were obtained in CH sections S3–S2 and S2–S1 and RT in boreholes S3, S2 and S1.

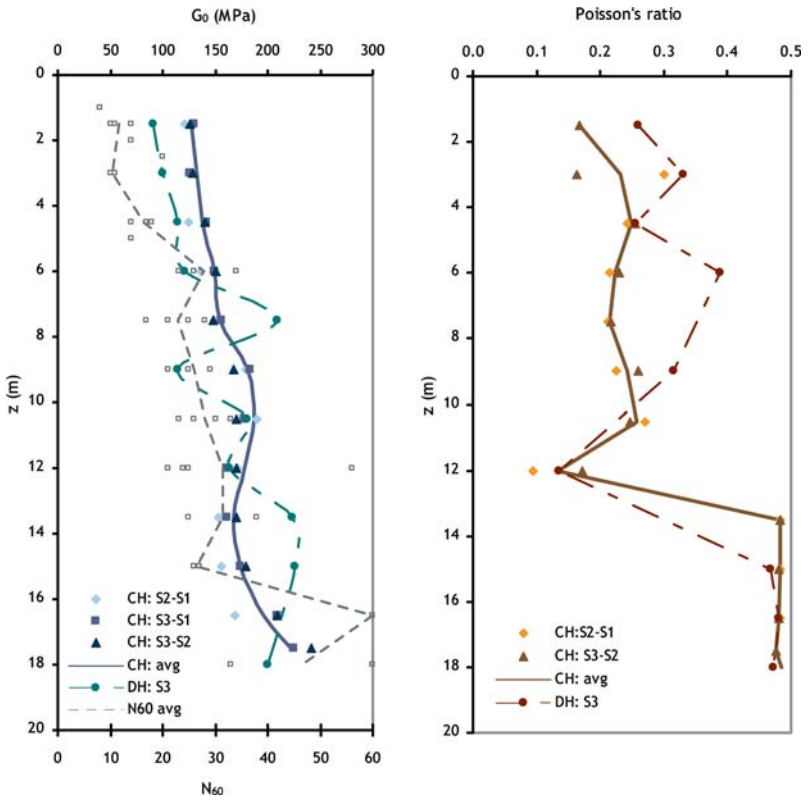

Figure 19. Shear modulus and Poisson ratio from CH sections and DH in borehole S3.

The highest G_0 values are located in borehole S1 showing increasing divergence with depth. The lowest ν values are located in borehole S1. The remaining ν sets have a similar trend mainly after 4.5 m depth with values around 0.25.

4.2. CLASSIFICATION BASED ON MECHANICAL INDICES FROM IN-SITU TESTS RESULTS

Classification charts based on the piezocone (CPTU) results, such as those proposed by Roberston (1990) are presented in Figure 21, reflecting considerable dispersion in the material type, as this evaluation may be conditioned by unreliable pore pressure measurements.

This general trend identifies this material as cemented and aged, with a grain size distribution from silty clays to clayey sands. Lab tests over recoiled samples have confirmed it mainly as clayey silty sand, when the analysis is made by classical wetting sieving and sedimentation with no use of chemical deflocculation (Viana da Fonseca et al., 2004).

The results presented above, obtained by means of a laser beam analyser, confirm the dominant class trend of silty sands, with very low clay fraction.

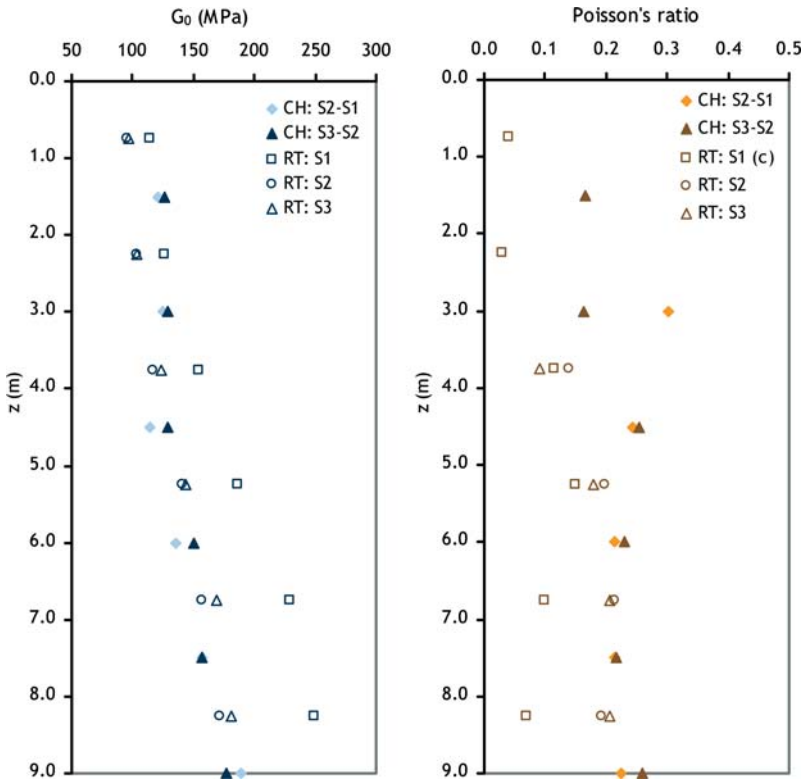

Figure 20. Shear modulus and Poisson's ratio from CH sections and "boreholes" RT.

Another classification based on the CPTU results has been introduced by Eslami and Fellenius (1997), mainly directed to pile design but also useful for geotechnical purposes. In Figure 22, this chart is presented together with the results of FEUP experimental site.

After application of both classification proposals to the piezocone results in depth, Costa (2005) generated the following profiles, confirming that this profile is ruled by a typical heterogeneity of residual soils (Figure 23).

The most surprising trend is the prevailing incidence of clayey matrices, which is not in accordance to the grain size distribution defined in laboratory tests. This diatomic behaviour was also explored by other classifications, such as those proposed by Marchetti (1980) and Zhang and Tumay (1999), and turned out to be also divergent in the percentage of fines. Figure 24 illustrates the discrepancies observed for one of the profiles – that of CPTU8, DMT6 and DMT8 (very close to each other).

There is clearly an unsuitable classification, which evidences the specificity of these soils and the compulsory need to adapt most of the classical proposals, developed for transported soils, to residual profiles.

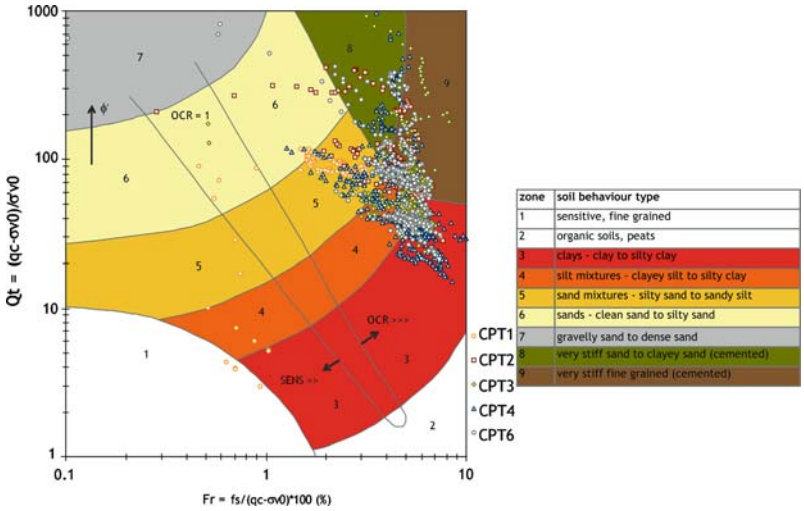

Figure 21. Soil behaviour classification chart (after Robertson, 1990).

This fact has been identified in other sites, a good example being the one described by Mayne and Brown (2002) referring to Piedmont residual soils. In this case, soils are comprised by fine sandy silts to silty fine sands, resulting from weathering of gneiss and schist. Classical classifications, such as the Unified Soils System, categorize these soils unsatisfactorily, since the definition of fine and coarse-grained groups are very much sensitive to such an extensive grain size distribution. The authors refer to similar contradictions in ID indices, such as stress history ratios, when comparing the results from lab tests over undisturbed samples and those inferred from in-situ tests (CPTU, DMT,...) results. These may be due to the specificity of the high degree of non-linearity, typical of these cemented soils, in very distinct patterns from the corresponding transported soils (with similar density and moisture content). The authors conclude that great care should be taken in using

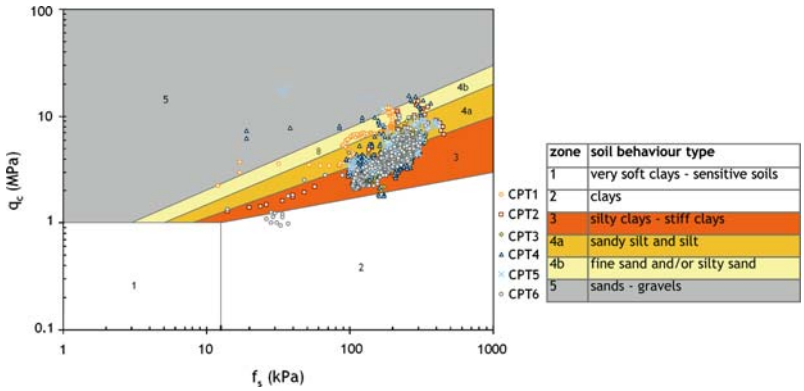

Figure 22. Soil behaviour classification chart (after Eslami and Fellenius, 1997).

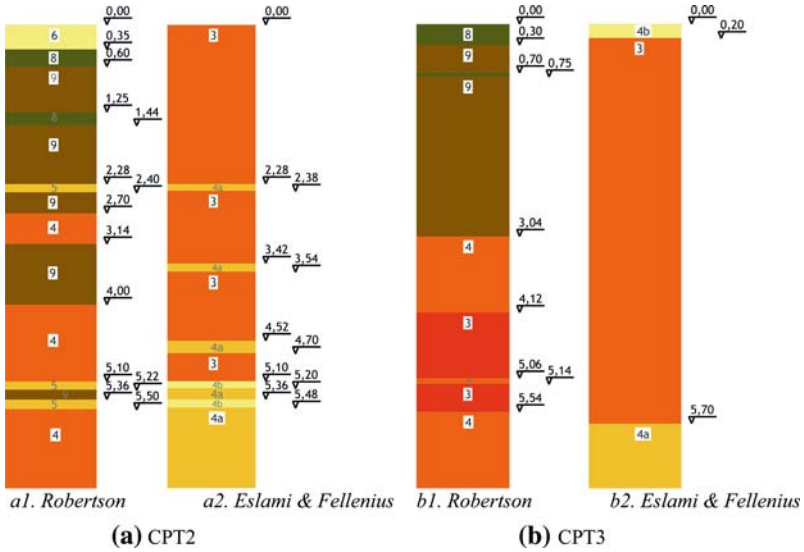

Figure 23. Soil behaviour classification profiles (Costa, 2005), based on the proposals of Robertson (1990) and Eslami and Fellenius (1997).

empirical correlations in non-textbook geomaterials, being necessary to verify design parametrical findings, by performing regional inter-crossing of experimental data (with emphasis to the use of comparison of calibration chambers and geotechnical structures prototypes tests results).

As stated by Schnaid et al. (2004), bearing in mind that soil classification using CPTU data is indirect and relies on empirical charts developed for strata interpretation, u_2

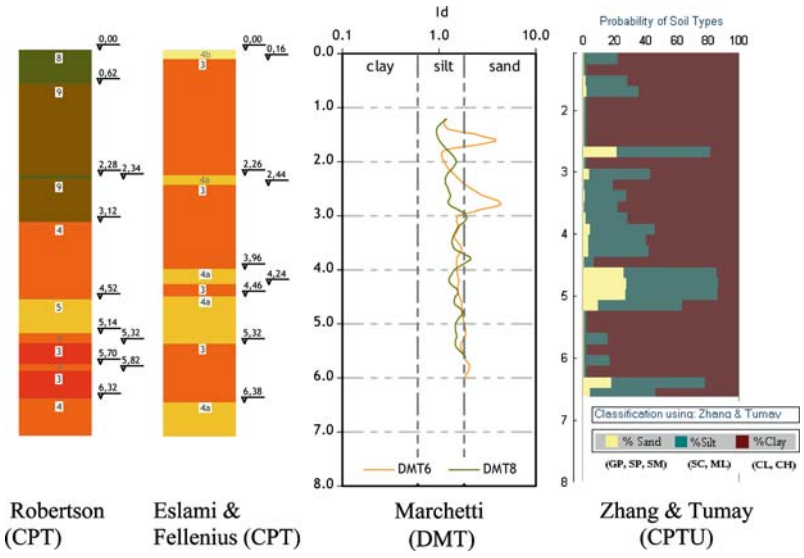

Figure 24. Profile identification from distinct tests based classifications.

measurements cannot always be considered useful to ensure a proper soil classification in unusual materials. Since classification charts should rely on at least two independent measurements, in the absence of pore pressure measurements, the authors suggest that q_c should be compared with the small strain stiffness G_0. The G_0/q_c ratio provides a measure of the ratio of elastic stiffness to ultimate strength and may therefore be expected to increase with ageing and cementation, primarily because the effect of these on G_0 is stronger than on q_c. Other authors, such as Bellotti et al. (1989), Rix and Stokoe (1992), Lunne et al. (1997) and Fahey et al. (2003) have reported, in sands, some new insights by correlating G_0/q_c versus q_{c1}, where q_{c1} is defined as:

$$q_{c1} = \left(\frac{q_c}{p_a}\right)\sqrt{\frac{p_a}{\sigma'_v}} \tag{1}$$

where p_a is the atmospheric pressure (note that the normalized parameter q_{c1} is dimensionless).

Once the profiles of q_c and G_0 are determined, these values can be directly used to evaluate the possible effects of stress history, degree of cementation and ageing for a given profile, as already recognised by Eslaamizaad and Robertson (1996). Data points are shown in Figure 25 for CPT tests carried out in residual soils (artificially cemented Monterey soils are also included), with specific emphasis to the values obtained for the FEUP experimental site (identified in the figure as "Porto, Portugal"). Since residual soils always exhibit some bond structure, the data fall outside

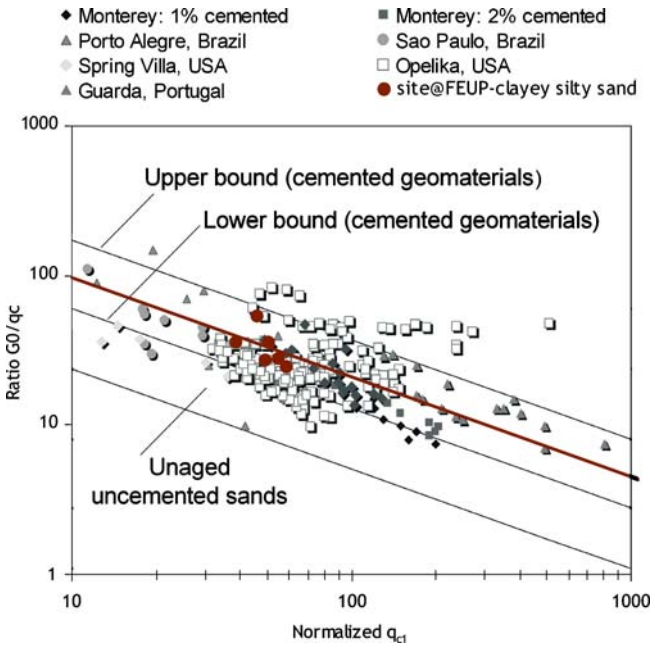

Figure 25. Relationship between G_0 and q_c for residual soils (Schnaid et al., 2004).

and above the band proposed by Eslaamizaad and Robertson (1996) as indicated in the figure.

The variation of G_0 with q_c observed in the range of sand deposits was expressed by upper and lower bounds. The upper bound for uncemented material can be assumed as a lower bound for cemented soils and a tentative new upper bound for cemented materials can be expressed as (Schnaid et al., 2004):

$$\left.\begin{array}{ll} G_0 = 800\sqrt[3]{q_c\sigma'_v p_a} & \text{upper bound; cemented} \\ G_0 = 280\sqrt[3]{q_c\sigma'_v p_a} & \text{lower bound; cemented} \\ & \text{upper bound; uncemented} \\ G_0 = 110\sqrt[3]{q_c\sigma'_v p_a}\ , & \text{lower bound; uncemented} \end{array}\right\} \quad (2)$$

The specific results of the present campaign (expressed in figure) may be expressed by:

$$G_0 = 450\sqrt[3]{q_c\sigma'_v p_a} \quad (3)$$

As for the CPT, Schnaid et al. (2004) point out that SPT N values can also be combined with seismic measurements of G_0 to assist in the assessment of the presence of bonding structure and its variation with depth. Such a combination is provided in Figure 26, which plots G_0/N_{60} against $(N_1)_{60}$ in residual soils, where $(N_1)_{60} = N_{60}\,(p_a/\sigma'_{v0})^{0.5}$ and is analogous to q_{c1} in Figure 25. Values of FEUP experimental site are also included. The bond structure is seen to have a marked effect on the behaviour of residual soils, with normalised stiffness (G_0/N_{60}) values considerably higher than those observed in cohesionless materials. A guideline formulation to compute G_0 from SPT tests may be given by the equations:

$$\frac{(G_0/p_a)}{N_{60}} = \alpha N_{60}\sqrt{\frac{p_a}{\sigma'_{v0}}} \quad \text{or} \quad \frac{(G_0/p_a)}{N_{60}} = \alpha(N_1)_{60} \quad (4)$$

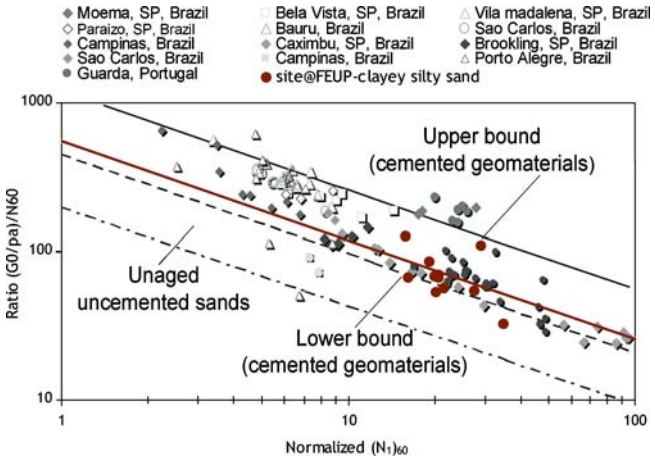

Figure 26. Correlation between G_0 and N_{60} for residual soils (Schnaid et al., 2004).

where α is a dimensionless number that depends on the level of cementation and age as well as on the soil compressibility and suction. The variation of G_0 with N can also be expressed by upper and lower boundaries, similarly to the cone penetration data (Schnaid et al., 2004):

$$\left.\begin{array}{rl} G_0 = 1200\sqrt[3]{N_{60}\sigma'_v p_a^2} & \text{upper bound; cemented} \\ G_0 = 450\sqrt[3]{N_{60}\sigma'_v p_a^2} & \text{lower bound; cemented} \\ & \text{upper bound; uncemented} \\ G_0 = 200\sqrt[3]{N_{60}\sigma'_v p_a^2} & \text{lower bound; uncemented} \end{array}\right\} \quad (5)$$

The specific results of the present campaign (expressed in figure) may be expressed by:

$$G_0 = 550\sqrt[3]{N_{60}\sigma'_v p_a^2} \quad (6)$$

It follows from the foregoing that a bonded/cemented structure produces G_0/q_c and G_0/N_{60} ratios that are systematically higher than those measured in cohesionless soils. These ratios therefore provide a useful means of assisting site characterization.

4.3. LABORATORY TESTS OVER UNDISTURBED SAMPLES

Undisturbed samples were carefully taken from the experimental site, in boreholes at specific depths, using high-quality piston samplers (Viana da Fonseca and Ferreira, 2002). The laboratory tests conducted in the first phase of the programme, comprised 6 CK_0D triaxial – 4 in compression with bender element (BE) readings and 2 in extension – with local strain measurements, 2 resonant column tests (RC), and 1 oedometer test. All specimens are identified in Table 4. A more thorough study is being conducted over block samples.

Figure 27 shows the particle size distribution of the tested specimens obtained from the undisturbed samples on borehole S2, and a typical grain size distribution fuse for Porto silty sand. According to the identification tests results, and with the results previously presented, the main composition of this saprolitic soil is a fine to medium grade and low plasticity material, mainly classified as silty sand (SM). The most representative physical properties for these samples of borehole S2 are presented over depth in Figure 28. More detailed geological and physical properties were presented for the whole soil profile in Section 2.

These laboratory tests focused mainly on triaxial tests. Stress–path and corresponding stress–strain curves are shown in Figure 29. At rest coefficient K_0 was taken as 0.50. Regional experience indicates even lower values (Viana da Fonseca and Almeida e Sousa, 2001).

From the analysis of tests results, the following strength parameters were obtained (specimen S2/3 was not considered due to some inconsistency):

$$\phi' = 45.8^\circ; \quad c' = 4.5\,\text{kPa}$$

The oedometer and resonant column tests curves, carried out on specimens from borehole S5, are presented in Figures 30 and 31.

Table 4. List of laboratory specimens, testing methods and

Specimen, depth (m)	γ kN/m^3	W%	ε	Sr%	w_L%	w_P%	<2 μm%	<#200%	<#10%	Testing method	σ'_{cv} (kPa)
S2/1(c), 3.2	18.2	16.3	0.72	62	32	27	5.3	38.5	85.0	Triaxial compression[1]	60.0
S2/2(e), 3.5	16.6	18.8	0.93	56	—	—	—	—	—	Triaxial extension[2]	60.0
S2/3(c), 4.0	18.4	16.2	0.75	61	44	27	9.5	47.2	74.4	Triaxial compression[1]	90.0
S2/4(e), 4.4	18.4	21.7	0.83	74	—	—	—	—	—	Triaxial extension[2]	80.0
S2/5(c), 5.5	19.0	22.5	0.71	86	NP	NP	7.7	41.2	82.5	Triaxial compression[1]	100.0
S2/6(c), 7.0	19.0	20.2	0.68	81	NP	NP	3.3	40.7	86.9	Triaxial compression[1]	140.0
S5/1, 4.0	20.0	13.8	0.50	74	—	—	—	—	—	Resonant column	80.0
S5/2, 6.3	17.8	22.1	0.82	73	—	—	—	—	—	Oedometer	—
S5/3, 8.0	19.0	19.7	0.66	80	—	—	—	—	—	Resonant column	160.0

– ASTM Sieves series.
(1) $CK_0(=0.5)D$ under stress controlled: $\sigma'_v \ll, \sigma'_h = \text{ctt}$, with measurement of V_S by bender elements.
(2) $CK_0(=0.5)D$ under strain–path controlled: $\sigma'_h \gg, \sigma'_v = \text{ctt}$.

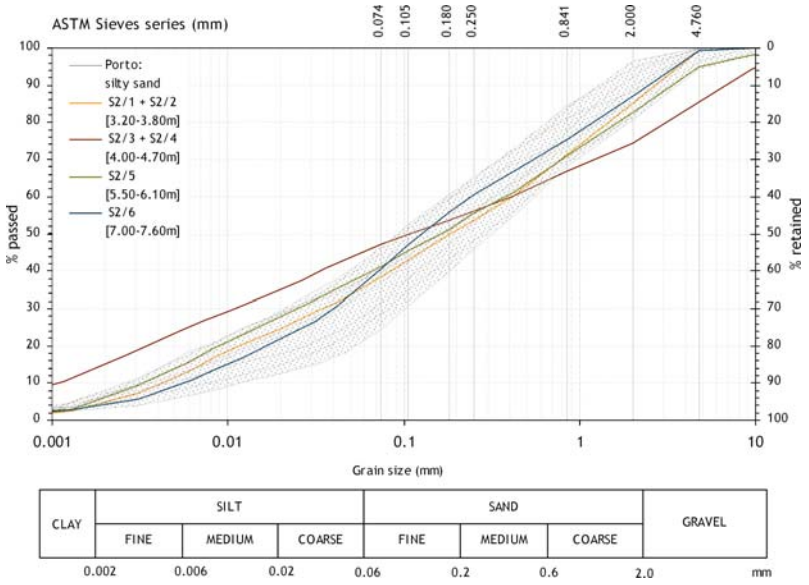

Figure 27. Grain size distribution curves from the experimental site, compared with Porto silty sand (Viana da Fonseca, 2003).

In the resonant column tests, the specimens were reconsolidated under anisotropic conditions for a stress level equal to the best estimate of the in-situ stresses (Table 1). The normalized stiffness and the damping ratio are plotted as a function of the shear strain in Figure 31. The evolution of the curves is similar to the ones obtained in sands (Santos, 1999).

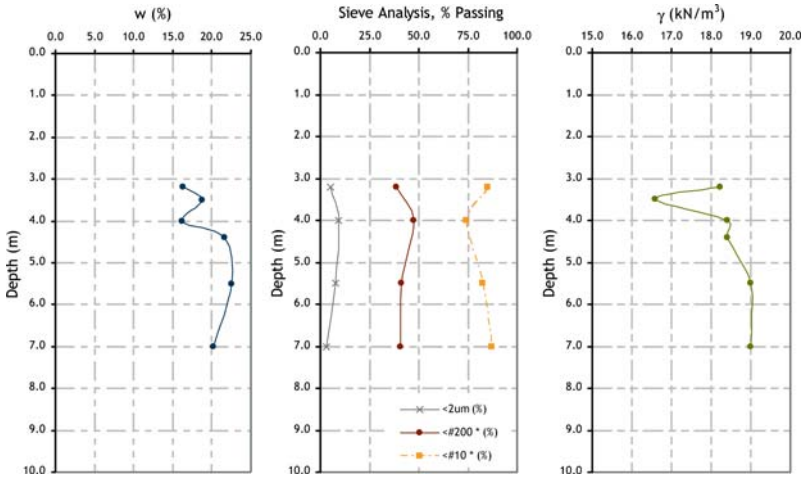

Figure 28. Soil index properties (borehole S2).

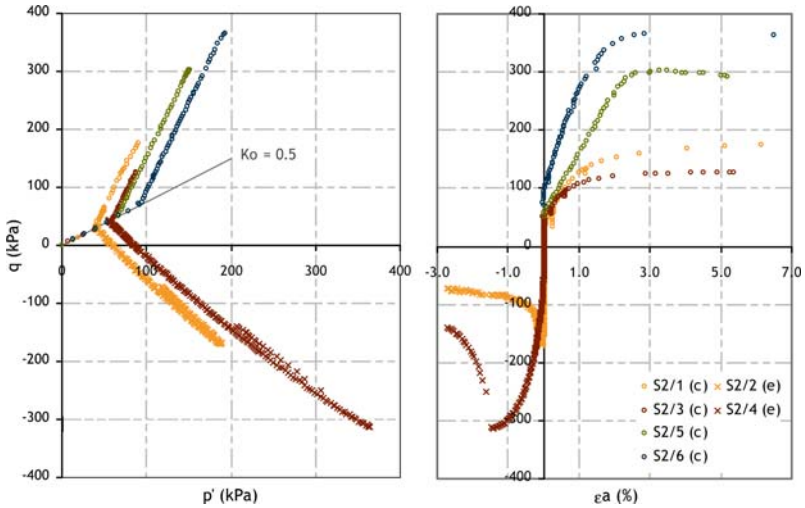

Figure 29. Triaxial tests: stress–path and stress–strain curves (compression and extension).

5. General Trends and Correlations between Tests

5.1. STRENGTH

Some correlations have been derived from the results database, and described elsewhere (Viana da Fonseca et al., 2004, Carvalho et al., 2004).

Values of $(N_1)_{60}$, taken from the SPT tests, allowed to derive the angle of shearing resistance from Décourt's (1989) proposal, ranging from 35° to 41°, with an average of 38°. This value coincides with those reported in similar regional soils, namely for Porto silty sand (Viana da Fonseca, 2003).

The classification chart by Robertson (1990) shows some dispersion (the chart was presented in Figure 21), but the general trend identifies this material as cemented and

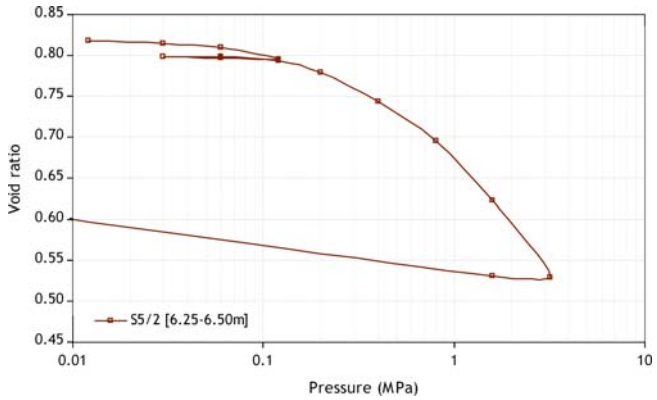

Figure 30. Oedometer test results: compressibility curve.

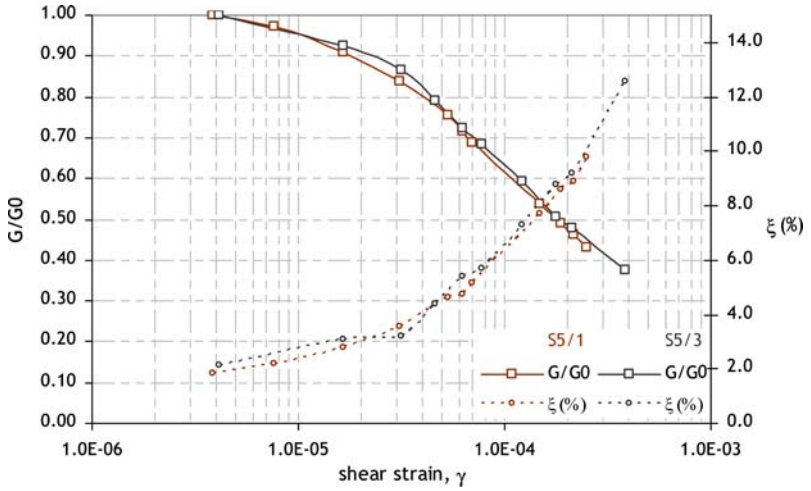

Figure 31. Resonant column results: normalized stiffness and damping ratio versus shear strain.

aged, with a grain size distribution from silty clays to clayey sands. Lab tests over recoiled samples have confirmed it mainly as clayey silty sand (Viana da Fonseca et al., 2004).

The relation between q_c from CPT and σ'_{v0} is presented in Figure 32, which integrates Robertson and Campanella's (1983) curves for the estimation of the angle of shearing resistance. The CPT results reveal a moderate increase of q_c in depth. Robertson and Campanella's proposal tends to lead to higher values of ϕ', especially

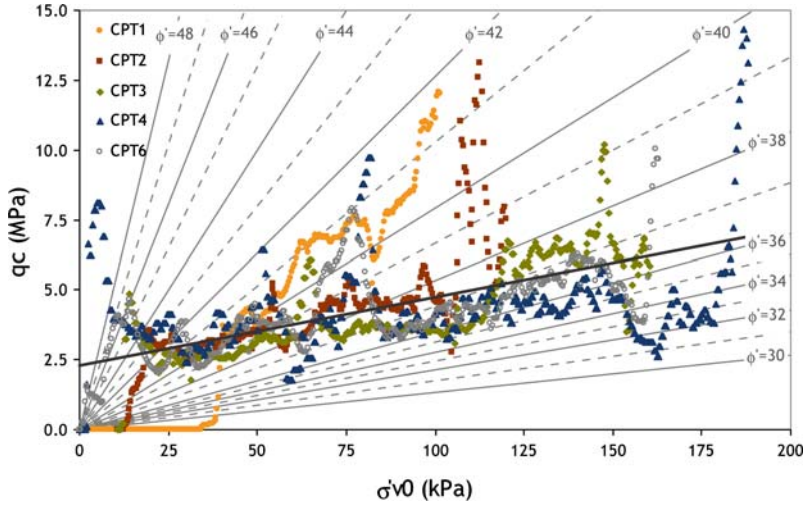

Figure 32. Relation between q_c values, in situ at rest effective stress, σ'_{v0}, and the angle of shearing resistance, ϕ' (Robertson and Campanella, 1983).

at lower depths, than those obtained from triaxial tests, since the effective cohesive component is not considered.

This reflects the simultaneous sensitivity of q_c towards frictional and cohesive components. In the present case, the CPT results are rather constant in depth, crossing a wide range of friction angles (35–42°) with more incidence at 37°, which is much lower than the one obtained in the laboratory tests. This can be a consequence of the behaviour of a cohesive-frictional soil, where the lower confinement levels are dominated by the cohesive component, while the higher are mostly governed by friction.

The usefulness of correlating results from SPT and CPT tests, led to the evaluation of q_c/N_{60} ratio and its dependence on the mean grain size, D_{50} (Robertson and Campanella, 1983). For the case of the experimental site, this ratio varied from 0.17 to 0.36 ($D_{50}=0.15$ mm – Figure 27). Different parent rocks generally produce different correlations for the same particle size distribution, due to intrinsic heterogeneity (Danzinger et al., 1998).

The Brazilian data show a general trend of lower values for the relation q_c/N_{60} with D_{50} than that expressed by Robertson and Campanella's (1983) average line. Data from FEUP experimental site are in close agreement with those results, but somewhat contradictory with Porto silty sand data, as illustrated in Figure 33. This discrepancy is probably a consequence of the more intensive clayey content of the soil in the present experimental site (see Figures 21 and 23).

Other reported values of the ratio q_c/N_{SPT} for different residual soils are indicated in Table 5, along with results from this experimental site. The percentage of fines has a clear influence in the obtained values.

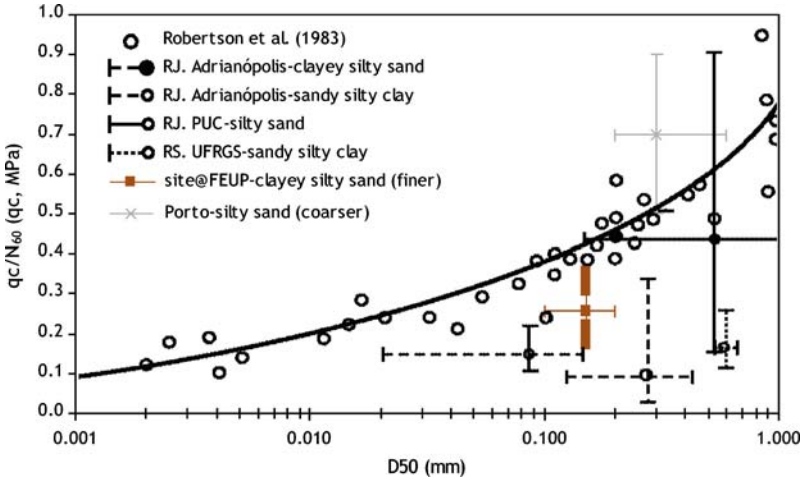

Figure 33. Ranges of q_c/N versus D_{50} on Brazilian residual soils, compared with the experimental site results (based on Danziger et al., 1998).

Table 5. Estimated values of q_c/N_{SPT} for different residual soils

Reference	q_c/N_{SPT} (q_c MPa)
Sandroni (1985) - Brazilian residual soils	0.30–0.78
Ajayi e Balogum (1988) - Nigerian saprolitic and lateritic tropical soils	0.40
Chang (1988) - Singaporean saprolitic granite soils	0.20
Viana da Fonseca (2003) - Porto silty sand (coarser)	0.50–0.90
FEUP experimental site - clayey silty sand (finer)	0.17–0.36

DMT and PMT results are not discussed in detail in this paper, but preliminary analyses of these test results have also enabled the soil identification. Nevertheless, as stated above – see Figure 24 – DMT I_d graph presented, classifies it as a silty sand to silt, which does corroborates the results of the identification tests (Figures 9 and 27; Tables 3 and 5) but which is not in accordance with the classification based on charts with input on penetration tests (CPT, CPTU,...).

It should be emphasized that the Dilatometer Test may be a very useful frame to evaluate the cohesive-frictional nature of these residual soils (Cruz et al., 2004). For this approach, the angle of shear resistance is determined from obtained results of DMT and CPTU tests by mean of Marchetti's (1997) and Robertson and Campanella's (1983) correlations. For the regional soils, a significant data has been collected and analysed, and, in general, the values of the parameter range from 35° to 45°, which are globally higher than those determined under controlled conditions in triaxial tests on undisturbed samples, if the cohesive fraction is not considered. Taking into account the low influence that sampling has on the evaluation of the angle of shear resistance, the registered difference on the value of ϕ' is attributed to the effects of the cementation structure on q_c and K_D parameters.

The methodology for the derivation of this cohesive component is described in Cruz et al. (1997) following a fairly simple way. Assuming that K_D reflects the overall strength of soil, it is expected that both c' and ϕ' have influence on this parameter. Then, if ϕ' deduced from triaxial testing is assumed, the corresponding K_D may be back-calculated. The difference between the two values of K_D (measured and back-calculated) will reveal the effective cohesive intercept. From available data, the cohesion obtained from DMT, c'_{DMT}, ranged from 5 to 15 kPa, which were

Table 6. Strength parameters from in-situ and laboratory tests

Tests		ϕ' [°]	c′ [kPa]
In situ	SPT	38	n/a
	CPT	37	n/a
	DMT	35–38	6–10
Laboratory	TX compression	45.8	4.5
	TX extension	28	12

confirmed by triaxial testing. A summary of the strength parameters, derived from in-situ and laboratory tests results is presented in the Table 6.

5.2. STIFFNESS – G_0 A "BENCHMARK"

The small strain shear modulus G_0 is the initial stiffness of the stress–strain curve for a given soil (Gomes Correia et al., 2004). This modulus, if properly normalised with respect to void ratio and effective stress, is in practical terms independent of the type of loading, number of loading cycles, strain rate and stress/strain history. It is then a fundamental parameter of the ground, considered as a benchmark value, which reveals its true elastic behaviour.

The results of shear wave CH tests are very consistent and reveal a rather smooth increase of G_0 with depth. The best linear fit with the overburden effective vertical stress is

$$G_0\,(\text{MPa}) = 127.8 + 218 \cdot \sigma'_{v0} \quad (R^2 = 0.83) \tag{7}$$

A representative value for the at rest coefficient $K_0 = 0.36$ can be assumed, based on regional experience (Viana da Fonseca and Almeida e Sousa, 2001); preliminary K_0 tests over two samples have confirmed this trend. Hence, the previous expression can be rewritten as a function of the mean effective stress, p'_0:

$$G_0\,(\text{MPa}) = 127.8 + 380 \cdot p'_0 \quad (R^2 = 0.83) \tag{8}$$

Viana da Fonseca (2003) proposed the following relation, for Porto silty sand:

$$G_0\,(\text{MPa}) = 98.5 + 230 \cdot p'_0 \tag{9}$$

Ishihara (1982) has compiled several proposals from different authors for the relationship between shear modulus and mean effective stress. Iwasaki and Tatsuoka (1977) proposed the following generic expression:

$$G_0\,(\text{kPa}) = A \cdot B \cdot F(e) \cdot (p'_0)^m \tag{10}$$

where

$$F(e) = \frac{(2.17 - e)^2}{1 + e} \tag{11}$$

For reconstituted clean sands containing no fines, A ranges from 14 300 to 16 600 B takes the value of 1 and the exponent m is equal to 0.4. For increasing percentages of fines, the value of B progressively decreases, up to a limit of 0.4 for about 20% fines.

Higuchi et al. (1981) and Kokusho and Esashi (1981) have applied the same generic relationship to undisturbed sandy soils and diluvial sands, respectively, deriving identical values of these parameters: $A = 14\,300$ to 7900 and $m = 0.4$ (B was not defined, i.e., the constant A is in fact A^*B). For undisturbed sands with 50% fines, Higuchi et al. (1981) have found values of A from 3090 to 2360 and $m = 0.6$.

In order to establish similar relations for the present soil, it is first necessary to define the void ratio function in depth. With the undisturbed samples recovered in

the experimental site, it was possible to determine the respective void ratios, shown in Table 2 and an estimate of its variation over depth was calculated, which provided a good correlation:

$$e = 0.783 \cdot \exp^{-0.019 \cdot z} \quad (R^2 = 0.63) \tag{12}$$

Having normalized the small strain shear modulus to the void ratio function, the initial proposal was rewritten, as follows:

$$\frac{G_0}{F(e)} = 110000 \cdot p_0'^{0.02} \tag{13}$$

It can be seen that the value of the constant for the small strain shear modulus expression is much higher for these residual soils ($A = 110000$) than for sandy transported soils, while the exponent m, reflecting the influence of the mean effective stress, is substantially lower.

For Porto silty sand, Viana da Fonseca (2003) found different constants, describing a slightly higher dependence of G_0 on the mean effective stress. This may result from the fact that the saturation conditions of these soils are significantly different. The comparison of these trends is presented in Figure 34.

$$\frac{G_0}{F(e)} = 65000 \cdot p_0'^{0.07} \tag{14}$$

Correlations between N_{SPT} and stiffness are very sensitive to different factors, while those relations between penetration parameters and small strain shear modulus (G_0) are somewhat independent of misleading factors, such as scale effects, non-linearity, etc. A simple but very useful power law between G_0 and N_{60} (Stroud, 1988) was

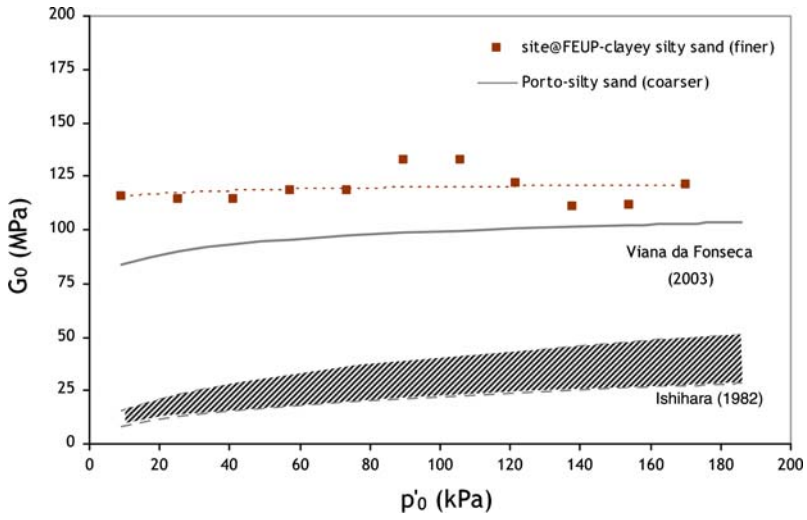

Figure 34. Comparison between observed and reference proposals of G_0 variation with effective stress.

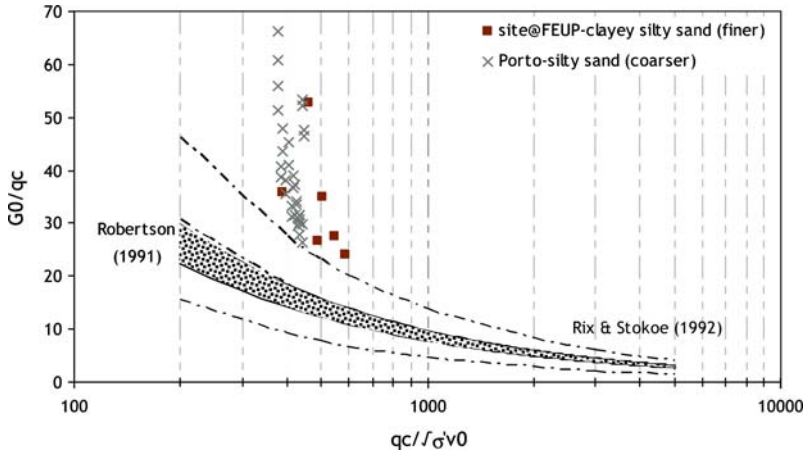

Figure 35. G_0/q_c versus $q_c/\sqrt{\sigma'_{v0}}$ from in-situ tests at FEUP experimental site, compared with other regional data and with reference curves.

obtained, where only the SPT results from the boreholes nearest to the CH tests (S1 and S3) were considered:

$$G_0\,(\text{MPa}) = 63 \cdot N_{60}{}^{0.30} \tag{15}$$

This expresses a stronger relation than that reported by Viana da Fonseca (2003) for Porto silty sand:

$$G_0\,(\text{MPa}) = 57 \cdot N_{60}{}^{0.20} \tag{16}$$

Jamiolkowski et al. (1988) showed that the same variables of soil density and in-situ effective stresses control both q_c and G_0. Hence, correlations between q_c and G_0 can be found for uncemented and unaged cohesionless soils (Robertson, 1991; Rix and Stokoe, 1992). These are framed with results from this experimental site and Porto silty sand in Figure 35.

This has obvious correspondence to the results expressed above, for G_0/N_{60} versus $(N_1)_{60}$ and G_0/q_c versus q_{c1}, in Figures 25 and 26. Cementation and ageing have different influences over q_c and G_0, which allows for the identification of ''unusual'' soils such as highly compressible sands, cemented and aged soils and clays with either high- and low-void ratio. As stated in Section 4.3, this particular relation between stiffness and penetration resistances (both in q_c and N_{60}) constitutes a step towards classification, as well as another way of correlating these values for parametrical deduction. That is, once a pattern of correlation is obtained, such as those in Equations (3) and (6), the value of this benchmark stiffness (G_0) can be reliably evaluated for design purposes.

In-situ seismic V_S obtained in CH tests and measured in the laboratory, with bender elements or in the resonant column (very close values), are compared in Figure 36. The similarity of V_S trends in depth from both in-situ and laboratory tests

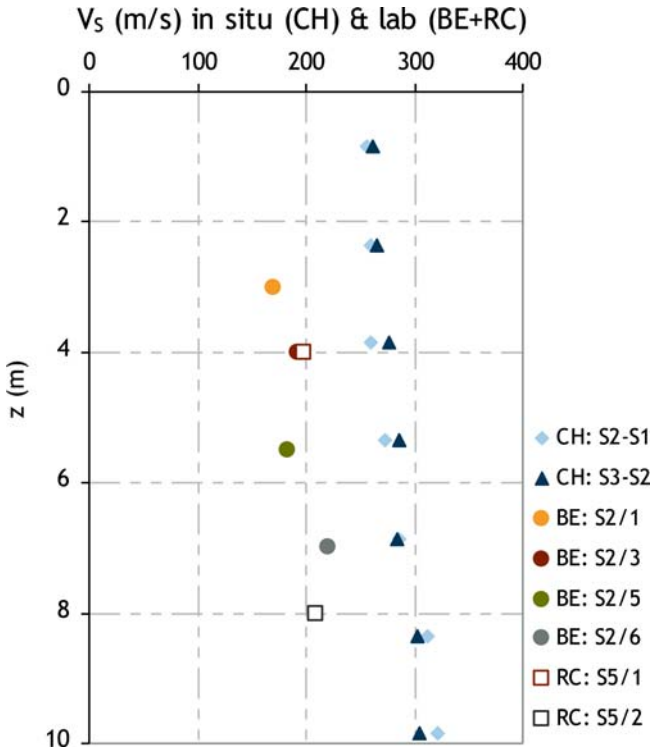

Figure 36. V_S profiles from in-situ and laboratory tests.

is evident and the differences encountered may well be mainly due to the disturbances associated with the sampling processes. These residual soils are particularly sensitive to sampling, since their behaviour is strongly controlled by the structure inherited from the parent rock.

These issues relating to sensitivity to sampling processes were discussed in detail in Viana da Fonseca and Ferreira (2002). Ageing may also explain why velocity of body waves of natural deposits of some age differ from that of same soil in laboratory with the same state of effective stress and void ratio.

5.3. AN EXPLORATORY BIVARIATE REGRESSION ANALYSIS

Some of the calculated G_0 values were used in an exploratory uni- and bivariate regression analysis with N-SPT values and depth. Both field N_{SPT} values, from boreholes S3 and S1, as well as the corresponding corrected values, N_{60}, were used.

Figures 37 and 38 show the calculated and predicted G_0 values from CH section S3–S2 based on N-SPT values from borehole S3 and depths between 1.5 and 15 m.

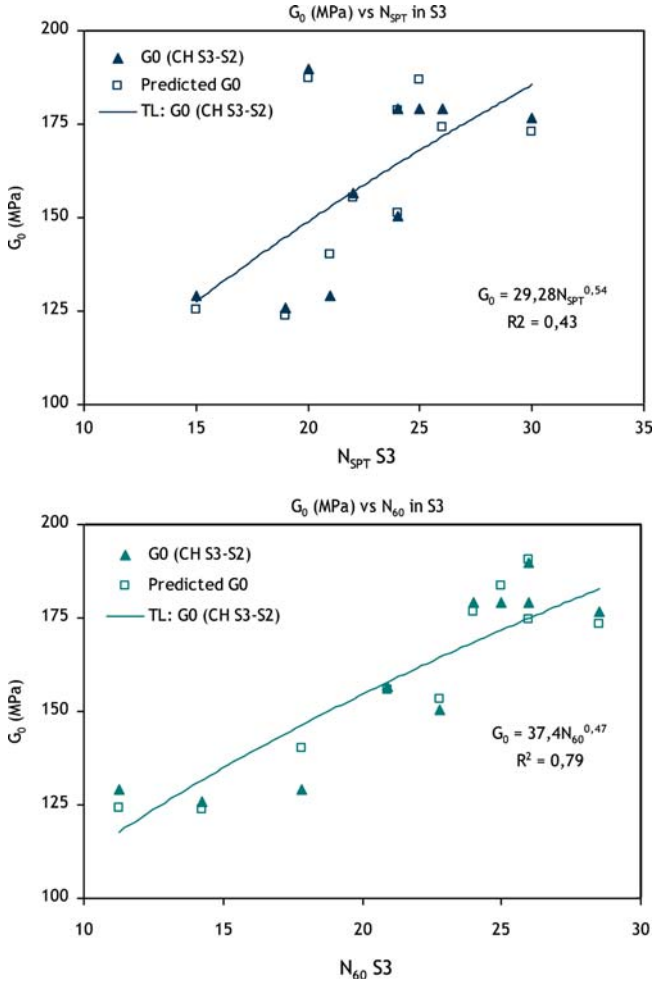

Figure 37. G_0 from CH S3–S2 versus N_{SPT} and N_{60} in S3 and depth. Trend lines for calculated G_0: $G_0 = 29.3N_{SPT}^{0.54}$ and $G_0 = 37.4N_{60}^{0.47}$.

The bivariate linear regression models coefficients used to calculate the predicted G_0 values are shown in Table 7 while in Table 8 the univariate power regression models coefficients used to calculate the G_0 trend line are presented.

The following equations represent the bivariate linear regression model for G_0 estimation based in both N-SPT values and depth:

- For G_0 from CH S3–S2 and N_{60} in S3:

$$G_0 = 95.2 + 1.6N_{60} + 3.5z \tag{17}$$

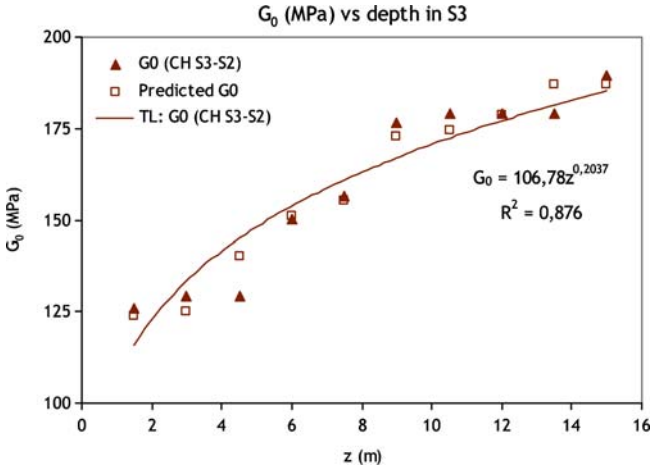

Figure 38. G_0 from CH S3–S2 versus depth. Trend line for calculated G_0: $G_0 = 106.8 \quad z^{0.20}$.

- For G_0 from CH S2–S1 and N_{60} in S1:

$$G_0 = 75.6 + 4.5N_{60} - 1.6z \tag{18}$$

As referred in Table 7 the related multiple squared correlation coefficient values, $M{\cdot}R^2$, respectively 0.98 and 0.92, are significantly higher than those obtained with univariate regression power models.

Table 7. G_0 bivariate linear regression models

Coefficients		Std. error	$M \cdot R^2$
CH S3–S2			
Intercept	91.5	11.1	0.95
Depth	4.6	0.5	
N_{SPT}-S3	1.3	0.5	
Intercept	95.2	8.7	0.98
Depth	3.5	0.7	
N_{60}-S3	1.6	0.6	
CH S2–S1			
Intercept	54.3	23.6	0.84
Depth	−0.8	2.5	
N_{SPT}-S1	4.9	1.7	
Intercept	75.6	17.2	0.92
Depth	−1.6	2.8	
N_{60}-S1	4.5	1.6	

Table 8. G_0 univariate power regression models

	N_{SPT}	N_{60}
CH S3–S2		
Coef.	29.3	37.4
power	0.54	0.47
R^2	0.43	0.79
CH S2–S1		
Coef.	26.5	44.4
power	0.58	0.42
R^2	0.83	0.82

6. Conclusions

The extensive site investigation/characterization carried out at the University of Porto experimental site has enabled the determination of the most relevant geotechnical properties of this soil profile, as well as deriving and comparing the obtained correlations with other proposals referring to residual soils from granite. The study allowed an insight at the distinctive particularities, in geological and geotechnical terms, of young residual soils (saprolitic) from granite that dominate most geotechnical profiles in and around Porto, in Northern Portugal.

This paper summarizes the generic trend of surface and borehole mechanical and geophysical in-situ tests applied to ground characterization and mapping. It also presents and discusses the obtained results, giving emphasis to the correlations encountered between the different tests, specific to saprolitic soils with weak relic structures. Both laboratory and in-situ tests results have assisted in characterizing deformability and strength of residual soils. Specific concepts for classification and characterization have to be used, taking into account micro and macrofabric analyses, which have strong consequences on the behaviour of these soils, to be clarified.

The integration of the information obtained from the experimental data (in-situ and lab), in terms of stiffness and strength, to assess the methods used for geotechnical design considering the behaviour of these specific soils, has been made through new parametrical correlations.

Several in-situ testing techniques were used, namely penetration tests: SPT and CPTU; pressure-dilatometer tests: PMT and DMT; seismic: conventional and tomographic refraction, reflection, CH and DH, electrical imaging, ground probing radar. These have provided a very comprehensive knowledge of the mechanical characteristics of the soil. Undisturbed samples were retrieved and an extensive laboratory testing program was carried out, including oedometric consolidation tests, CK0D triaxial tests using local strain measuring devices and bender-extender elements, as well as resonant column tests. This residual saprolitic soil from granite

was classified, under classical terms, as clayey silty sand and this assumption is supported by the results of the various tests.

One of the relevant conclusions is the high spatial variability correlation presented by seismic and electrical imaging section models as well as the very consistent similar horizontal interface pattern common to interpretative models from seismic stacked section, conventional refraction and GPR radargram. In addition, the SH wave velocity fields (CH, reflection and refraction) and resistivity model supports the local geological evidence.

The resulting refraction, mostly tomographic, and electrical models point out to the adequacy of both methods in mapping the local underground heterogeneities, both horizontally and vertically, inside the more or less weathered granitic mass as well as the boundary with the gneissic migmatite.

Tentative geological interpretation models integrating information, namely from S-wave refraction, high-resolution shallow reflection and GPR surveys, are also presented.

Acknowledgments

The authors are grateful to the Private Sponsors of this experimental site: Mota-Engil, SA, Sopecate, SA; Tecnasol-FGE, SA, and Teixeira Duarte, SA. This work was developed under the research activities of CEC from the FEUP and ICIST of IST, supported by multi-annual funding from FCT (Portuguese Science and Technology Foundation).

References

Ajayi, L.A. and Balogun, L.A. (1988) Penetration testing in tropical lateritic and residual soils – Nigerian experience. Penetration Testing – 1988. In: De Ruiter (ed.), *Proceedings of the ISOPT-1*, Vol. 1, Orlando. A.A. Balkema Pub., Rotterdam, pp. 315–328.

Almeida, F., Hermosilha, H., Carvalho, J.M., Viana da Fonseca, A. and Moura, R. (2004) ISC'2 experimental site investigation and characterization – Part II: From SH waves high resolution shallow reflection to shallower GPR tests, In: Viana da Fonseca A. and Mayne P.W. (eds.), *Geotechnical and Geophysical Site Characterization*, 1 Millpress, Rotterdam, pp. 419–426.

Carvalho, J.M., Viana da Fonseca, A., Almeida, F. and Hermosilha, H. (2004) ISC'2 experimental site invest. and characterization – Part I: Conventional and tomographic P and S waves refraction seismics vs electrical resistivity, In: Viana da Fonseca A. and Mayne P.W. (eds.), *Geotechnical and Geophysical Site Characterizaton*, 1 Millpress, Rotterdam, pp. 433–442.

Chang, M.F. (1988) In-situ testing of residual soils in Singapore. In: *Geomechanics in Tropical Soils*. Proc. Sec. Int. Conf., Vol. 1, Singapore. A.A. Balkema Pub., Rotterdam, pp. 97–108.

Costa, E. (2005) Tests and response analysis of piles in residual soils from granite under vertical loads. *MSc Thesis, University of Porto*, Portugal (in Portuguese).

Cruz, N., Viana da Fonseca, A., Coelho, P. and Lemos, J. (1997) Evaluation of geotechnical parameters by DMT in Portuguese soils. In: *Proceedings of the XIV Int. Conf. on Soil Mechanics and Foundation Engineering*. Balkema, Rotterdam, pp. 77–80.

Cruz, N., Viana da Fonseca, A. and Neves, E. (2004) Evaluation of effective cohesive intercept on residual soils by DMT data, In: Viana da Fonseca A. and Mayne P.W. (eds.), *Geotechnical and Geophysical Site Characterizaton*, 2 Millpress, Rotterdam, pp. 1275–1278.

Danzinger, F.A.B., Politano, C.F. and Danzinger, B.R. (1998) CPT-SPT correlations for some Brazilian residual soils. In: *Proceedings of the First Int. Conf. on Site Characterization – ISC'98*. Atlanta, Vol. 2, Balkema, Rotterdam, pp. 907–912.

Décourt, L. (1989) The standard penetration test. State of the Art Report. In: *Proceedings of the XII ICSMFE*, Vol. 4, Rio de Janeiro. Balkema, Rotterdam, pp. 2405–2416.

Eslaamizaad, S. and Robertson, P.K. (1996) A framework for in-situ determination of sand compressibility. In: *Proceedings of the 49th Canadian Geotechnical Conference*, St John's Newfoundland.

Eslami, A. and Fellenius, B.H. (1997) Pile Capacity by Direct CPT and CPTU Methods Applied to 102 Case Histories, *Can. Geotech. J.*, **34**, 886–904.

Gomes Correia, A., Viana da Fonseca, A. and Gambin, M. (2004), Routine and advanced analysis of mechanical in-situ tests. In: Viana da Fonseca A. and Mayne P.W. (eds.), *Geotechnical and Geophysical Site Characterization*, Keynote Lecture, Vol. 1, Millpress, Rotterdam, pp. 75–95.

Higuchi, Y., Umehara, Y. and Ohneda, H. (1981) Evaluation of dynamic properties of the sand deposits under deep seabed. In: *Proceedings of the 36th Annual Convention, JSCE*, Vol. 3, pp. 50–51.

Ishihara, K. (1982) Evaluation of soil properties for use in earthquake response analysis. In: *Proceedings of the International Symposium on Numerical Models in Geomechanics*, pp. 237–259.

Iwasaki, T. and Tatsuoka, F. (1977) Effects of grain size and grading on dynamic shear moduli of sands, *Soils and Foundations*, **17**(3), 19–35.

Jamiolkowski, M., Ghionna, V.N, Lancellota, R. and Pasqualini, E. (1988) New correlations of penetration tests for design practice. In: De Ruiter (ed.), *Proceedings of the ISOPT-1*, Vol. I, Orlando. Balkema, Rotterdam, pp. 263–296.

Kokusho, T. and Esashi, Y. (1981) Cyclic triaxial test on sands and coarse materials. In: *Proceedings of the 10th International Conference on Soil Mechanics and Foundation Engineering*, Vol. 1, Stockholm, pp. 673–679.

Lunne, T., Robertson, P.K. and Powell, J.J.M. (1997) *Cone Penetration Testing in Geotechnical Practice*, Blackie, London.

Marchetti, S. (1980) *In situ tests by flat dilatometer*, *J. Geotech. Eng. Div., ASCE*, **106, GT3**, 299–321.

Marchetti, S. (1997) The Flat Dilatometer Design Applications. In: *Proceedings of the III Geotechnical Engineering Conference*, Cairo University.

Mayne, P.W. and Brown, D.A. (2002) Site characterization of Piedmont residuum of North America. In: *Characterization and Engineering Properties of Natural Soils*, Vol. 2, Swets & Zeitlinger, Lisse, pp.1323–1339.

Pearce, J.A., Harris, N.B.W. and Tindle, A.G. (1984) Trace element discrimination diagrams for the tectonic interpretation of granitic rocks, *J. Petrol.*, **25**, 956–983.

Pereira, E. (1992) Geological Map of Portugal, on Scale 1:200,000, Sheet n.1., INETI, Porto (in Portuguese).

Ribeiro, A., Marcos, A., Pereira, E., Llana-Fúnez, S., Farias, P., Fernández, F.J., Fonseca, P., Chaminé, H. and Rosas, F. (2003) 3-D strain in the Ibero-Armorican Arc: a review. Ciências da Terra (UNL), Lisboa, no. esp. V: 54–55.

Ribeiro, A., Quesada, C. and Dallmeyer, R.C. (1990) Geodynamic evolution of the Iberian Massif. In: Dallmeyer, R.D. and Martinez Garcia, E. (eds.), *Pre-Mesozoic Geology of Iberia*. Springer-Verlag, Berlin, pp. 399–410.

Rix, G.J. and Stokoe, K.H. (1992) *Correlations of Initial Tangent Modulus and Cone Resistance*, Elsevier, Potsdam, New York, pp. 351–362, Proceedings of the International Symposium on Calibration Chamber Testing.

Robertson, P.K. (1990) Soil classification using the cone penetration test, *Can. Geot. J.*, **27**, 151–158.

Robertson, P.K. (1991) Estimation of foundation settlements in sand from CPT. *ASCE Geot. Special Pub*. **II**(27), 764–778.

Robertson, P.K. and Campanella, R.G. (1983) Interpretation of cone penetration tests. Part I: Sand; Part II: Clay, *Can. Geot. J.*, **20**(4), 718–745.

Sandroni, S.S. (1985) Sampling and testing of residual soils in Brazil, In: Brand and Phillipson (eds.), *Sampling and testing of Residual Soils. A Revue of International Practice*, Scorpion Press, Hong Kong, pp. 31–50, Tech. Com. Samp. Test. of Residual Soil, ISSMFE.

Santos, J.A. (1999) Soil characterisation by dynamic and cyclic torsional shear tests. Application to the study of piles under lateral static and dynamic loadings. PhD Thesis, Technical University of Lisbon, Portugal (in portuguese).

Schnaid, F., Fahey, M. and Lehane, B. (2004) In situ test characterisation of unusual geomaterial, In: Viana da Fonseca A. and Mayne P.W. (eds.), *Geotechnical and Geophysical Site Characterization, Keynote Lecture*, Millpress, Rotterdam, pp. 49–74.

Stroud, M.A. (1988) *The Standard penetration test – its application and interpretation*, Thomas Telford, London, pp. 24–49, Proceedings of the Geot. Conference on Penetration Testing in U.K., Birmingham.

Viana da Fonseca, A. (2003) Characterizing and deriving engineering properties of a saprolitic soil from granite, in Porto, In: Tan, et al. (eds.), *Characterization and Engineering Properties of Natural Soils*, Swets & Zeitlinger, Lisse, pp. 1341–1378.

Viana da Fonseca, A. and Almeida e Sousa, J. (2001) At rest coefficient of earth pressure in saprolitic soils from granite, *Proceedings of the XIV ICSMFE, Istanbul*, **1**, 397–400.

Viana da Fonseca, A. and Ferreira, C. (2000), Management of sampling quality on residual soils and soft clayey soils. Comparative analysis of in situ and laboratory seismic waves velocities. In: *Proceedings of the Workshop Sampling Techniques for Soils and Soft Rocks and Quality Control*. FEUP, Porto (in Portuguese).

Viana da Fonseca, A., Carvalho, J., Ferreira, C., Tuna, C., Costa, E. and Santos, J. (2004) Geotechnical characterization of a residual soil profile: The ISC'2 experimental site, Porto, In: Viana da Fonseca A. and Mayne P.W. (eds.), *Geotechnical and Geophysical Site Characterizaton*, 2 Millpress, Rotterdam, pp. 1361–1370.

Zhang, Z. and Tumay, M.T. (1999) Statistical to fuzzy approach toward CPT soil classification, *ASCE J. Geotech. Geoenvir. Eng.*, **125**(3), 179–186.